International Journal of Biological Macromolecules 146 (2020) 387–404

Contents lists available at ScienceDirect

International Journal of Biological Macromolecules

journal homepage: http://www.elsevier.com/locate/ijbiomac

Exploring the nature of interaction and stability between DNA/RNA base pairs and defective & defect-dopant graphene sheets. A possible insights on DNA/RNA sequencing

Vinnarasi Saravanan, Akilan Rajamani, Saranya Vasudevan, Shankar Ramasamy *

Department of Physics, Bharathiar University, Coimbatore 641046, Tamil Nadu, India

ARTICLE INFO

Article history:
Received 4 September 2019
Received in revised form 7 November 2019
Accepted 1 January 2020
Available online 7 January 2020

Keywords:
Defective and defect-dopant graphene sheet
Si and B dopant
DFT
DNA/RNA sequencing
Bio-sensor

ABSTRACT

A quantum chemical investigation is performed to understand the adsorption behaviour of DNA/RNA base pairs onto the defective (Di-Vacancy (DV) and Stone-Wales (SW)), boron (B) and silicon (Si) defect-dopant graphene (B-DV, Si-DV, B-SW, and Si-SW) sheets using density functional theory (DFT). The stability of DNA/RNA base pairs on the Si-SW sheet is found to be −80.59 kcal/mol (G-C), −70.21 kcal/mol (A-T), and −69.78 kcal/mol (A-U). The quantum theory of atoms in molecule (QTAIM) analysis concluded that the interaction of DNA/RNA base pair on Si-SW sheet has partially electrostatic and partially covalent (Si···N) characters. The natural bond orbital analysis (NBO), electron density difference map (EDDM), and natural population analysis (NPA) are revealed that the charge has been transferred from DNA/RNA base pair to defective and defective-dopant graphene sheet. From the time-dependent density functional theory (TD-DFT), a strong redshift is observed at 482 nm for GC-Si-SW, 494 nm for AT-Si-SW, and 497 nm for AU-Si-SW. Hence, the substantial variations in the HOMO-LUMO gap (ΔE_{HL}) and UV spectra of Si-SW sheet after the adsorption of DNA/RNA base pair can be beneficially exploited to design a new bio-sensor or DNA/RNA sequencing devices.

1. Introduction

Deoxyribonucleic acid (DNA) is the predominant genetic material in the incarnating realm [1] and it is a large biomolecular structure that is made up of four different nitrogenous chemical. Each nitrogenous base are combined together (A-T and G-C) to form long double strands spiral structure that called as DNA double helix. An important nucleic acid along with DNA is ribonucleic acid (RNA) which translates genomic evidence from DNA to proteins [2]. Both DNA and RNA are notable because they can both encode genetic instructions and retain attracted properties, comprising the capability to bind precise targets [3]. In recent years, DNA and RNA sequence recognition has received much attention due to its auspicious applications in various fields such as disease diagnoses and treatment, forensic analysis, food safety assessment, environmental observing, pharmaceutical application, and so on [4]. There are plenty of two dimensional (2D) and one dimensional (1D) hybrid materials are extensively used to recognize the order of DNA and RNA sequence. The interaction of DNA and RNA sequence with hybrid materials have long been a considered process relevant to the genesis of life.

Understanding the interaction of DNA, RNA and protein with carbon-related materials is very essential for emerging novel hybrid materials that could have a wide range of applications in biomolecular recognition [5], self-organization to molecular electronics and drug delivery [6–11]. Remarkably, nucleic acid (DNA and RNA) and protein with carbon-related materials share a synergetic correlation. Graphene, graphene oxide and its derivative have excellent properties and concomitant applications in biosensor, engineering, energy storage, field-effect transistor (FET), catalysis, biology and medicine [12–17]. Due to the large surface area, the graphene can facilitate the adsorption of biomolecules and gas molecules [18–20]. Functionalized (covalent and non-covalent) graphene and carbon nanotubes (CNT) were used to discriminate the different nucleotides in the sequencing of DNA [21–24] and it can be used for the deduction of pesticides and pollutants [25,26]. The recognition of adsorbed biomolecules on the graphene is feasible due to its high conductivity and charge transfer mechanism between biomolecules and graphene material [27]. The doping of graphene with atoms (B, N, Si, Al, P, and S) is an effective way to increase its chemical reactivity and also enhance the adsorption strength between molecules and graphene [28,29]. Recently Xiangkai Kong et al. [30] reported, while compared to pristine graphene, both B-doping and hydrogen-decorated at the edge of the graphene sheets act as a better catalyst for oxygen reduction reaction (ORR) in fuel cells. Sun et al. [31] have been found that the B doped carbon nanotube (CNT) enhances the adsorption strength of biomolecules. The B-dopant atom modifies the structural, electronic and chemical properties of pristine

* Corresponding author.
E-mail address: rshankar@buc.edu.in (S. Ramasamy).

https://doi.org/10.1016/j.ijbiomac.2020.01.001
0141-8130/

graphene sheet, thus it could be used for biomolecular identification and separation technology [32]. Previous studies have shown that the silicon (Si) atom doped with graphene sheet is used as a gas sensor for detecting NO and NO_2 molecule [33] and it plays as an effective and metal-free catalyst in the reduction of N_2O gas molecule [34,35]. S. K. Mudedla et al. [36] have found that doping of Si atom can change the structural, electronic and optical properties of graphene sheet and it led to higher binding affinity towards biomolecules than the pristine graphene sheet. The high electrical conducting nature of graphene is altered into semiconductor with the doping of Si atom in graphene [36] and it increases the adsorbent nature of graphene sheet. Further, the presence of defects on graphene structure may alter the significant influences on the physical and chemical properties of graphene surface [37] since the defects can produce non-equivalent carbon atoms on the graphene surface. The most regular defects of graphene structure contain monovacancies, di-vacancies (DV), pentagon heptagon pairs (55-77), and adatom due to making of graphene from the thermal extension of graphite oxide (GO) [38]. D. Borisova et al. [39] suggested that the defective DV (5-8-5) graphene sheet is highly preferred than the mono-vacancy graphene sheet owing to its reconstruction of graphene without dangling bond [39]. Numerous gas molecules such as O_2, CO, CO_2, SO_2, N_2, and H_2O are chemically adsorbed on the DV graphene sheet with a magnitude of 3–13 eV adsorption energy [20,40,41]. Previous theoretical [38] investigation reported that DNA nucleobases interacted with DV sheet has higher binding affinity than pristine graphene and it could be used as a DNA sequencing application. Yong-Hui Zhang et al. [41] have found that stone-wales (SW) sheet could be an outstanding candidate as selective material for NO_2 gas molecule while compared to pristine graphene sheet. In particular, the Al doped at the reactive site of SW (55-77) sheet is more sensitive than the pristine graphene for the detection of formaldehyde (H_2CO) gas molecule [42]. This investigation clearly exposed that the presence of defect enhances the adsorption in the graphene sensors. The pristine graphene, doped graphene (B, N, Si, and so on) and DV graphene on biomolecules (DNA/RNA nucleobases and base pairs) adsorption mechanism have been analyzed previously. However, the effect of defective (SW) and defect-dopant (B-DV, Si-DV, B-SW, and Si-SW) combination on biomolecules (G-C, A-T and A-U base pairs) adsorption mechanism has not been addressed yet. Noticeably, it is significant to expose the binding nature of the defective and defect-dopant combination stack with DNA/RNA base pairs in biomedical application because the defective and defect-dopant combination site of graphene could give rise to a local electronic structure around it.

Hence, in the present study, the DFT simulation is performed to explore the adsorption mechanism of G-C, A-T, and A-U base pairs on the DV, B doped DV (B-DV), Si doped DV (Si-DV), SW, B doped SW (B-SW) and Si doped SW (Si-SW) graphene sheet. The strength of the H-bond energies and distortion energies are calculated for DNA/RNA base pair on defective and defect-dopant graphene sheet. The total adsorption is calculated for complex system using fragmentation method with basis set superposition error (BSSE) correction. The $\rho(r)$, $\nabla^2\rho(r)$, and H(r) parameters are used to understand the bond strength and nature of interaction between intermolecular complexation. Further, the aromatic character is explored for the pyrimidine and imidazole rings of base pairs by multicenter bond order (MCBO) index. The charge transfer process is also calculated for bare defective and defect-dopant graphene sheet and DNA/RNA base pair on defective and defect-dopant graphene sheet using NPA charge analysis, NBO, DOS, and EDDM analysis. The optical properties of the defective and defect-dopant graphene sheet are investigated after the adsorption of DNA/RNA base pair using TD-DFT method.

2. Computational details

Density functional theory (DFT) based functions such as M06-2X [43] and wB97XD [44] along with 6-311+g* basis set is extensively used for structural, electronic and energetic properties of weakly bounded systems. Thus, these functional and basis set are chosen for this present investigation. All the theoretical calculations are done by the DFT level of theory in Gaussian 09 program package [45]. The initial structure of G-C, A-T and A-U base pairs is optimized at the M06-2X and wB97XD level of theories. The DV and SW graphene structures are taken from the previous theoretical study [20]. The DV and SW graphene structure contains 40 (5-8-5) and 42 (55-77) carbon atoms and the edges are passivized with hydrogen atoms. The chemical formula for both DV and SW is $C_{40}H_{16}$ and $C_{42}H_{16}$. Further, DV and SW graphene structures are doped with boron (B) and silicon (Si) atom. The defective graphene sheet and defect-dopant combination of graphene sheets are optimized at the above level of theories. The base pairs stacking with defective and defect-dopant graphene sheets are also optimized at the same level of theory. The fragmentation energies of base pairs with defective and defect-dopant graphene sheets are corrected for basis set superposition error correction (BSSE) using counterpoise method suggested by Boys and Beradi [46]. The fragmentation energies are calculated using this equation [47,48]

$$\Delta E_{Total} = E_{ABC} - [E_A + E_B + E_C] \quad (1)$$

$$\Delta^3 E_{(ABC)} = \Delta E_{Total} - \left[\Delta^2 E_{(AB)} + \Delta^2 E_{(AC)} + \Delta^2 E_{(BC)}\right] \quad (2)$$

$$\Delta^2 E_{(AB)} = E_{AB} - \left[E_{(A)} + E_{(B)}\right] \quad (3)$$

where E_{ABC} represents the total energy of the complex system (base pair + defective and defect-dopant graphene sheet), E_A and E_B indicates the energy of the individual bases and E_C indicates energy of the defective and defect-dopant graphene sheet.

The hydrogen bonding energies of base pair in the presence and absence of defective and defect-dopant graphene sheets are evaluated using the below equation.

$$E_{HB}\ (BP) = E_{(BP)} - \left[E_{(Base\ 1)} + E_{(Base\ 2)}\right] \quad (4)$$

where E (BP), $E_{(Base\ 1)}$, and $E_{(Base\ 2)}$ mention that the energies of the optimized bare base pair and the single bases in the base pairs respectively.

$$E_{HB}\ (BP\ in\ complex) = E_{(BP\ in\ complex)} - \left[E_{(Base\ 1)} + E_{(Base\ 2)}\right] \quad (5)$$

Moreover, the distortion energy is calculated for the bare base pairs and base pairs in a complex system as given by

$$E_{dis} = E_{HB}\ (BP) - E_{HB}\ (BP\ in\ complex) \quad (6)$$

where E_{HB}(BP) denotes the energy of the bare base pairs in its optimized structure and E(BP in a complex system) represents the energy of base pairs in the complex system.

The NBO analysis is performed out to understand the charge transfer mechanism on defective and defect-dopant graphene sheet with DNA/RNA base pairs at the M06-2X/6-311+G* level of theory. The QTAIM is used to distinguish both covalent and non-covalent interaction between molecules. The MCBO index is calculated for DNA/RNA base pair after the adsorption on defective and defect-dopant graphene sheet. The EDDM is also calculated for base pairs with defective and defect-dopant graphene sheets. The sensitivity behaviour of defective and defect-dopant graphene sheet towards adsorption base pairs are further scrutinized by the density of states (DOS) and frontier molecular analysis (FMO). The TD-DFT method also used to calculate the optical sensing property of base pairs on the defective and defect-dopant graphene sheets.

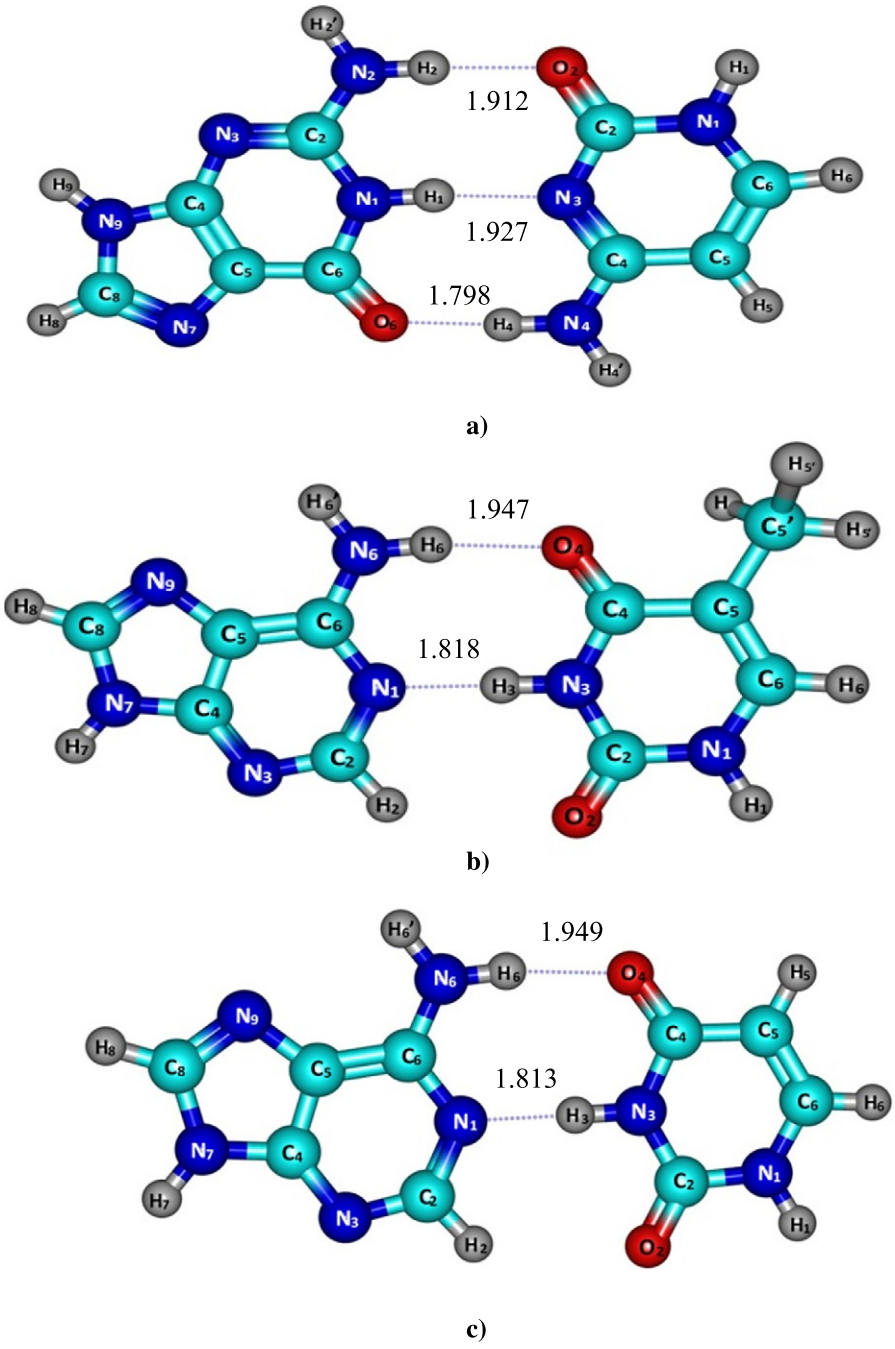

Fig. 1. The optimized structure of DNA/RNA base pairs. a) G-C, b) A-T, and c) A-U are optimized at M06-2X/wB97XD and 6-311+g* level of theories.

3. Results and discussion

3.1. Geometrical analysis

3.1.1. Structural properties of defect and defect-dopant graphene sheet

The main aim of the present work is to explore the interaction of DNA/RNA base pairs on DV, B-DV, Si-DV, SW, B-SW, and Si-SW graphene sheet using the DFT level of theory. All the theoretical simulations are done by the M06-2X functional with 6-311+g* basis set.

The optimized structure of DV, B-DV, Si-DV, SW, B-SW, and Si-SW graphene sheets are portrayed in Figs. 2 and 3, the corresponding bond distance is given in the Supplementary Table S1. The DV graphene sheet consists of two pentagon rings and one octagon (5-8-5) ring and it adopts non-planar arrangement which is shown in Fig. 2. The SW sheet contains two pentagon and two heptagon rings (55-77) and it can form

Table 1
Bond distance and bond angles are calculated for bare base pair using M06-2X with 6-311 +g* level of theory.

Base pairs	Bonding type	Distance (Å)	Angle (°)
A-T	N_3-H_3···N_1	1.818 [1.869][a]	179.2 [178.4][e]
	N_6-H_6···O_4	1.947 [1.926][a]	172.2 [174.6][e]
	N_1-H_1··· N_3	1.927 [1.988][b]	175.1 [176.1][c]
G-C	N_2-H_2··· O_2	1.912 [2.019][b]	176.6 [178.1][c]
	N_4-H_4···O_6	1.798 [1.916][b]	176.3 [177.0][c]
A-U	N_3-H_3···N_1	1.813 [1.806][d]	179.2
	N_6-H_6···O_4	1.949 [1.959][d]	171.7

[a] Ref. [81].
[b] Ref. [55].
[c] Ref. [82].
[d] Ref. [56].
[e] Ref. [50].

planar shape which is portrayed in Fig. 3. In DV sheet, the C—C bond distance variations are found to be in the range of 1.393 Å–1.419 Å (pentagon ring) and 1.409 Å–1.546 Å (octagon ring), these bond distance variations are compared with previous result [20]. The bond angle of two pentagon ring (C9-C11-C10 & C13-C14-C12) in DV sheet is calculated at 107.8° and this result is quite favoured with previous study (107.7°) reported by Shuaiwei Wang et al. [49]. Similarly, in the SW graphene sheet, the bond distance variations of C—C atoms are obtained at 1.388 Å–1.468 Å for pentagon ring and 1.333 Å–1.460 Å for heptagon ring and this result in good agreement with the previous report [50]. The C—C bond distance of the DV and SW graphene sheets slightly deviate around 0.05 Å −0.12 Å when compared to C—C bond distance of pristine graphene (1.340 Å) sheet [36], this is due to the presence of defects in a graphene structure [20]. Further, the B and Si atom are doped with defective graphene sheet and their optimized structures are given in Figs. 2b, c, 3b and c. When B and Si atom is replacing by a C atom in DV sheet, the C—C bond distance is elongated around 0.008–0.13 Å (B) and 0.27–0.33 Å (Si). In the case of SW sheet, the C—C bond distance is elongated around 0.02–0.05 Å (B) and 0.002–0.06 Å (Si) due to their high atomic radius of the B and Si atom than the C atom which is shown in Figs. 2 and 3. However, the planarity of SW sheet is not affected by the presence of B and Si dopant atom which is shown in Fig. 3. In the case of DV sheet, the B and Si atom is projected out from their basal plane because of its large atomic radius [51]

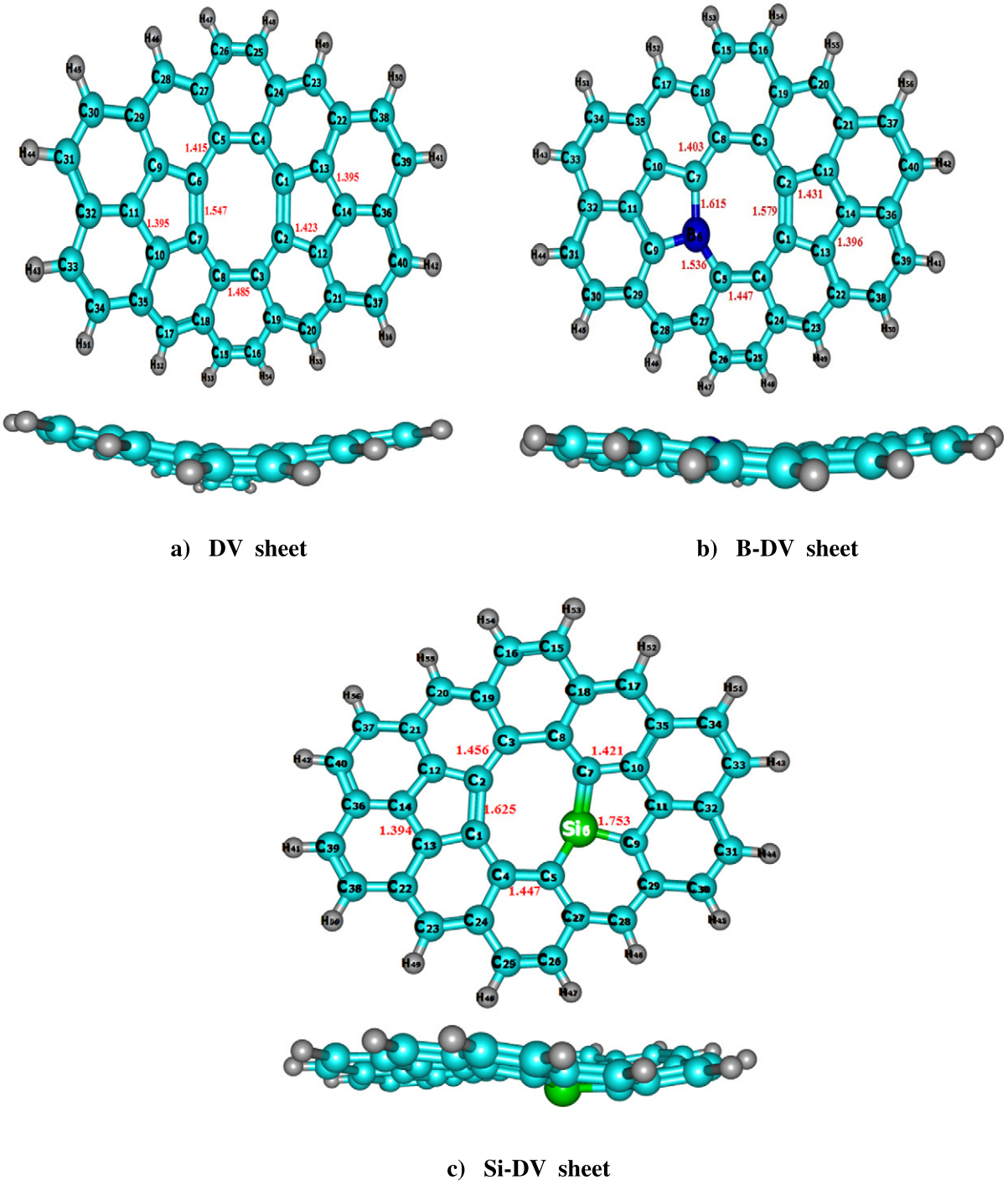

Fig. 2. The optimized structure of di-vacancy, boron (B) and silicon (Si) doped di-vacancy sheets are calculated using M06-2X and wB97XD with 6-311+g* level of theories.

which are depicted in Fig. 2. The B—C bond distance of DV and SW sheets are obtained at 1.548 Å and 1.530 Å, these results are good agreement with previous experimental (1.59 Å) [52] and theoretical (1.50 Å) results [53]. Similarly, the Si—C bond distance is found to be 1.752 Å for DV sheet and 1.717 Å for SW sheet and these values are also well correlated with previous theoretical (1.74 Å) value [36]. The calculated NPA (Mulliken charges (see Table S2)) atomic charges of C_5, C_7, and C_9 atoms of octagon and pentagon rings are found to be −0.358 eV (−0.274 eV), −0.364 eV (−0.279 eV), and 0.009 eV (0.004 eV) in DV sheet. Similarly, the atomic charge of C_1 and C_3 atoms of pentagon and heptagon rings are found to be −0.080 eV (−0.062 eV) and −0.215 eV (−0.118 eV) in SW sheet. The presence of B and Si dopant atom change the geometrical and electronic properties of DV and SW graphene sheet because of their high atomic radius. Due to the presence of dopant atom in the defective sheet, high charge transfer takes place from B and Si atom to C atom in both DV and SW sheet which is confirmed by the atomic charge analysis of NPA. While B doping in DV sheet the C_5, C_7, and C_9 atomic charges are increases from −0.274 eV to (−0.452 eV), −0.279 eV to −0.441 eV, and 0.004 eV to −0.331 eV. Correspondingly, the Si doped DV sheet, the C_5, C_7, and C_9 atomic charges are increased from −0.274 eV to −0.813 eV, −0.279 eV to −1.156 eV, and 0.009 eV to −1.105 eV. In the case of B doped SW sheet, the atomic charges increase from −0.062 eV to −0.361 eV (C_1 atom) and −0.118 eV to −0.399 eV (C_3 atom), similarly charge of Si doped SW sheet is increased from −0.062 eV to −0.820 eV (C_1 atom) and −0.118 eV to −1.000 eV (C_3 atom). When compared to B and Si

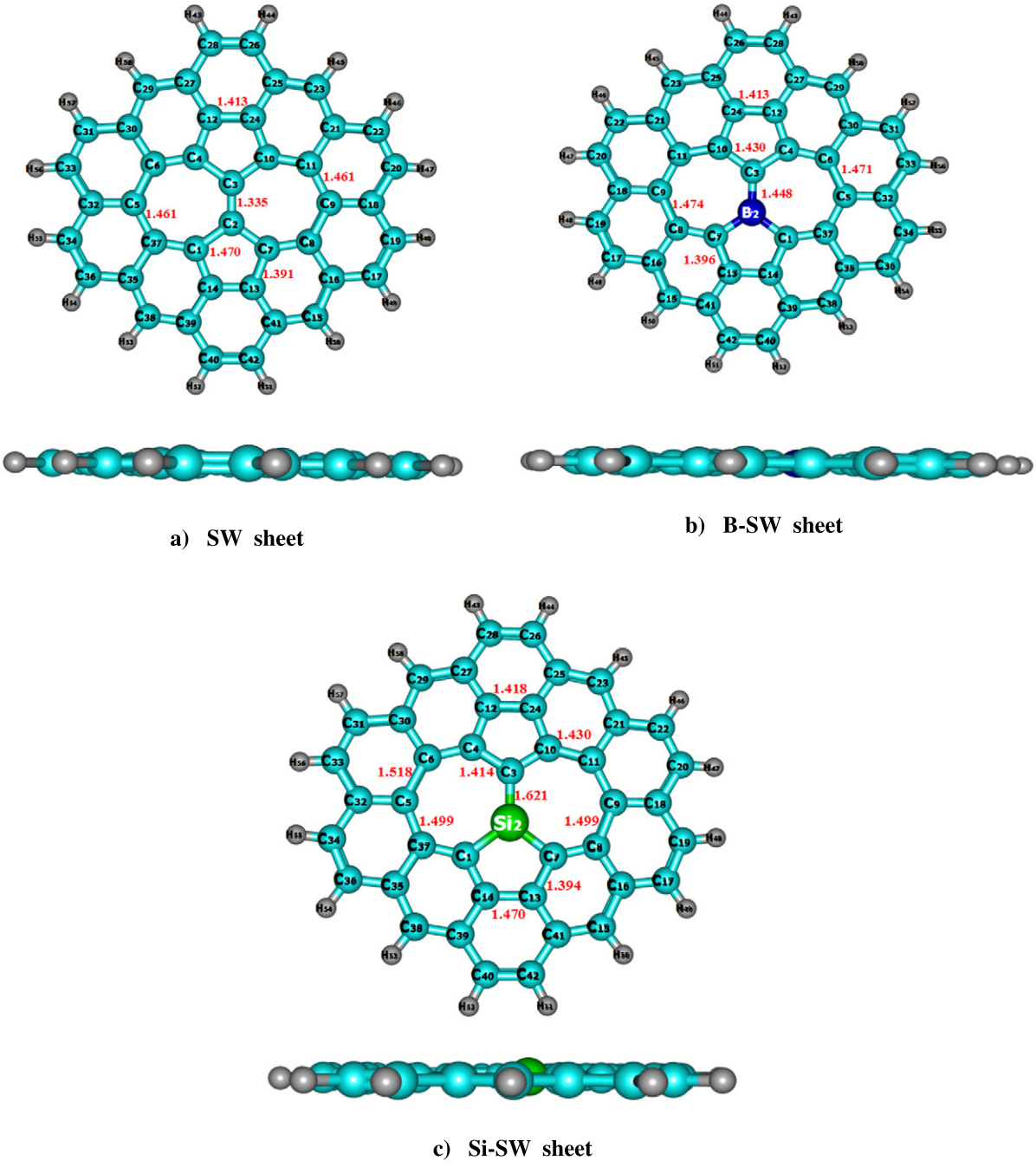

a) SW sheet

b) B-SW sheet

c) Si-SW sheet

Fig. 3. The optimized structure of stone-wale defect, boron (B) and silicon (Si) doped stone-wale (SW) defective sheets are calculated using M06-2X and wB97XD with 6-311+g* level of theories.

doped DV and SW sheet, the high charge transfer takes place from Si to C in SW sheet. Thus, the Si doped SW sheet is highly reactive and strongly adsorb DNA/RNA base pair than the Si and B doped DV sheet. Due to the high charge transfer, ΔE_{HL} values of DV sheet is reduced from 4.3 eV to 3.3 eV (B) and 3.8 eV (Si) for DV sheet. Similarly, in the case of SW sheet, the ΔE_{HL} reduced from 4.2 eV to 2.5 eV (B) and 4.0 eV (Si). These results revealed that the presence of dopant atom modifies the structural and electronic properties of defective graphene sheet and it highly adsorbs the DNA/RNA base pairs than the bare sheet [28].

3.1.2. Structural properties of bare base pairs and base pairs in complex

The normal DNA/RNA base pairs and DNA/RNA base pairs on defective and defect-dopant graphene sheets are optimized by M06-2X/6-311+g* level of theory. The H-bond interaction and vdW interactions are also calculated dispersion corrected DFT (DFT-D) based approach with wB97XD/6-311+g* level of theory. The initial structure of normal DNA base pairs is taken from the protein data bank (PDB ID: 1BNA) [54]. The optimized structure of A-T, G-C, and A-U are depicted in Fig. 1 and their H-bonding properties and energies are given in Table 1. The structural stability of A-T, G-C, and A-U base pairs are confirmed by

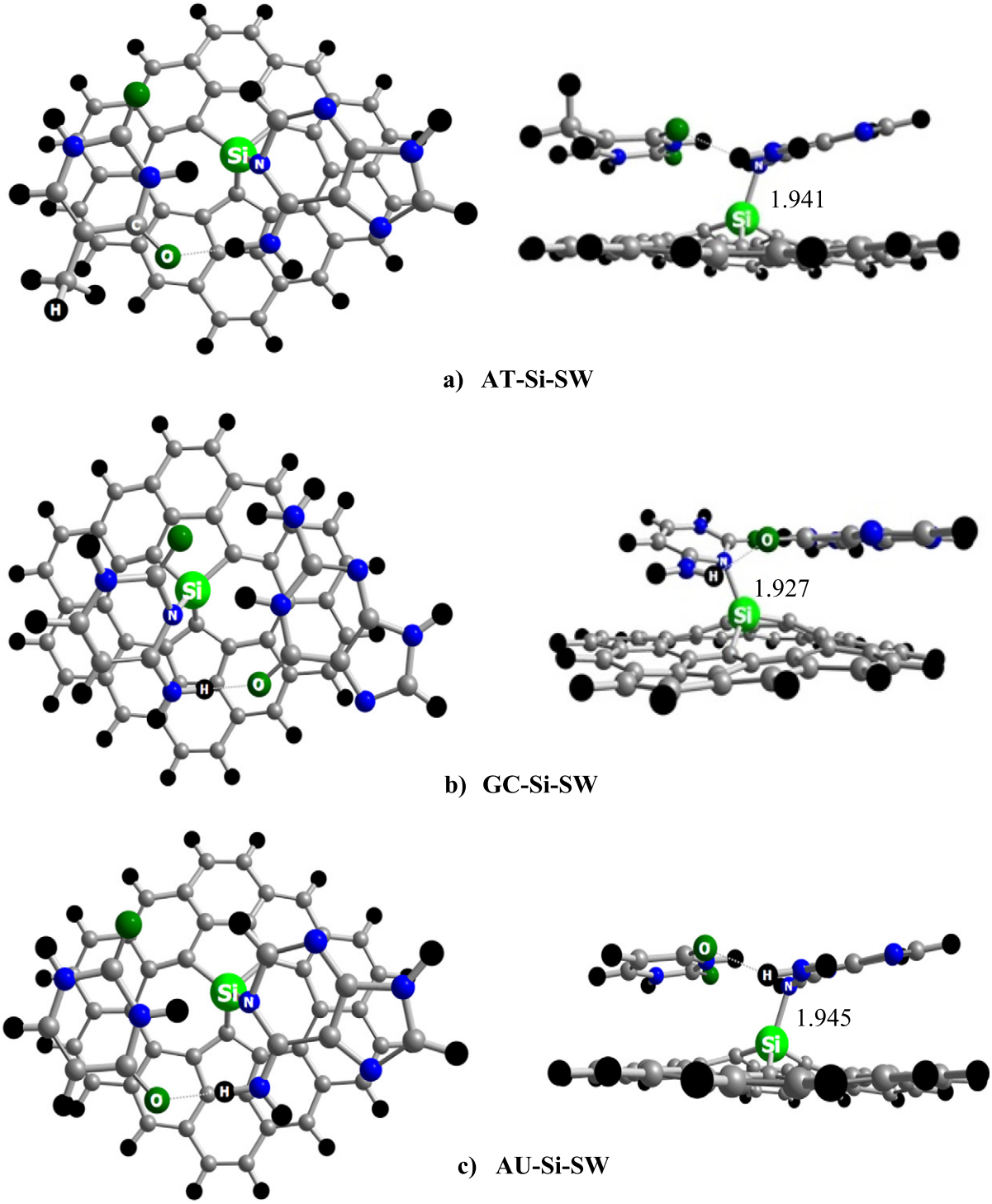

Fig. 4. The optimized structure of DNA/RNA base pairs on Si doped SW defective sheets are calculated using M06-2X and wB97XD with 6-311+g* level of theories.

vibrational frequency analysis. Herein, no imaginary frequencies are attained and it exhibits that the base pairs structure are all on real minima.

Fig. 1, A-T and A-U base pairs have two traditional H-bond interactions and G-C base pair has three H-bond interactions. In the optimized geometry of A-T and A-U base pairs, the amino group (NH_2) of H-atom (H_6) in the adenine residue is connected with a carbonyl group (C=O) of oxygen atom (O_4) in the thymine/uracil residue (N_6-H_6···O_4). Similarly, the N_3 position of H-atom (H_3) in the thymine/uracil residue is bonded with N_1 position of the adenine residue (N_3-H_3···N_1). The bond distance of N_3-H_3···N_1 is found to be 1.817 Å (A-T) and 1.810 Å (A-U), the corresponding bond angle is obtained at 179.3° (A-T) and 179.4° (A-U) respectively. Similarly, the N_6-H_6···O_4 bond distance is obtained at 1.920 Å (A-T) and 1.928 Å (A-U), bond angles are observed at 172.9° (A-T) and 173.1° (A-U) respectively. The obtained N_3-H_3···N_1 and N_6-H_6···O_4 bond distance are well related to previous reports [55,56].

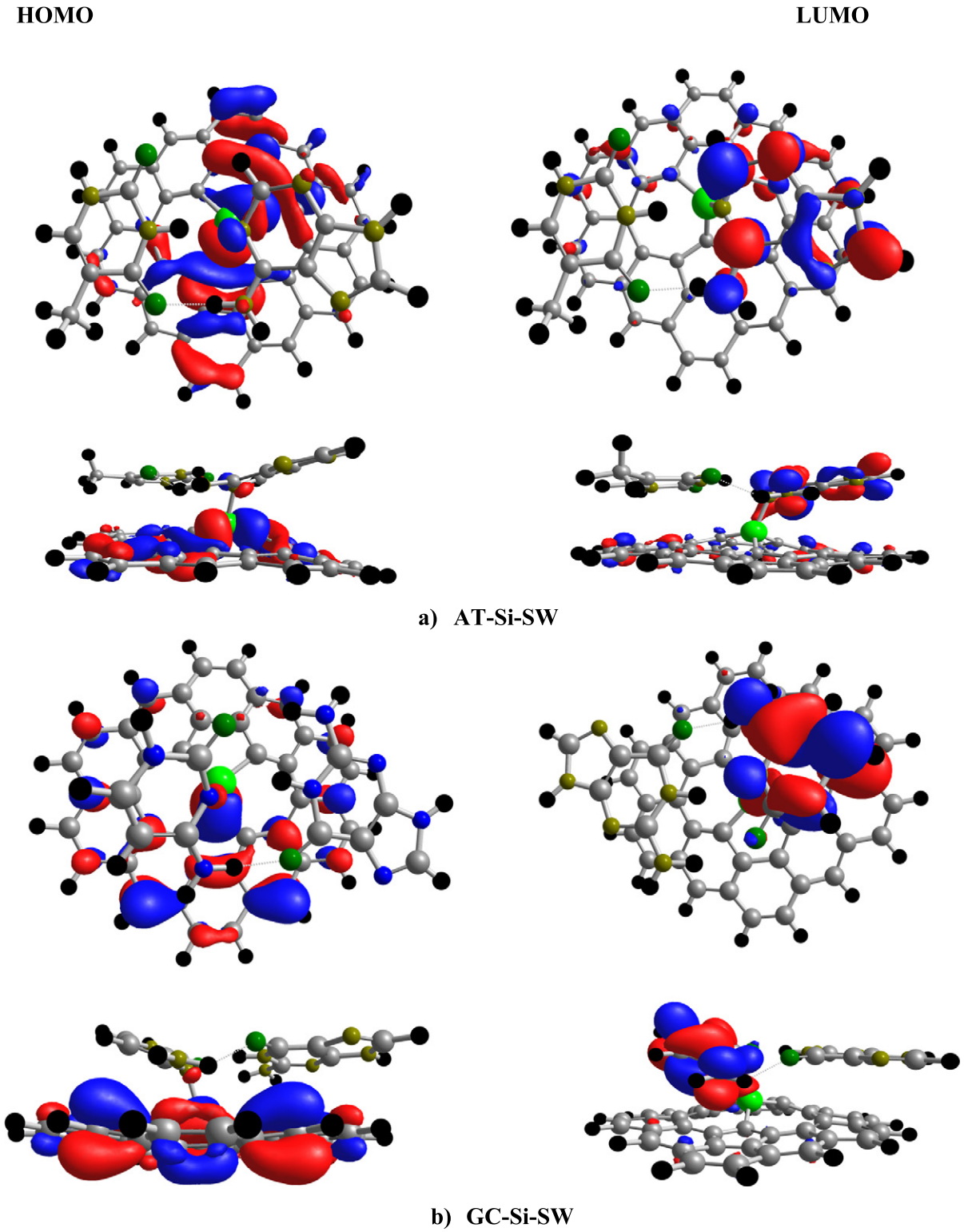

Fig. 5. HOMO and LUMO of DNA/RNA base pairs on Si doped SW defective sheets are calculated using M06-2X with 6-311+g* level of theory.

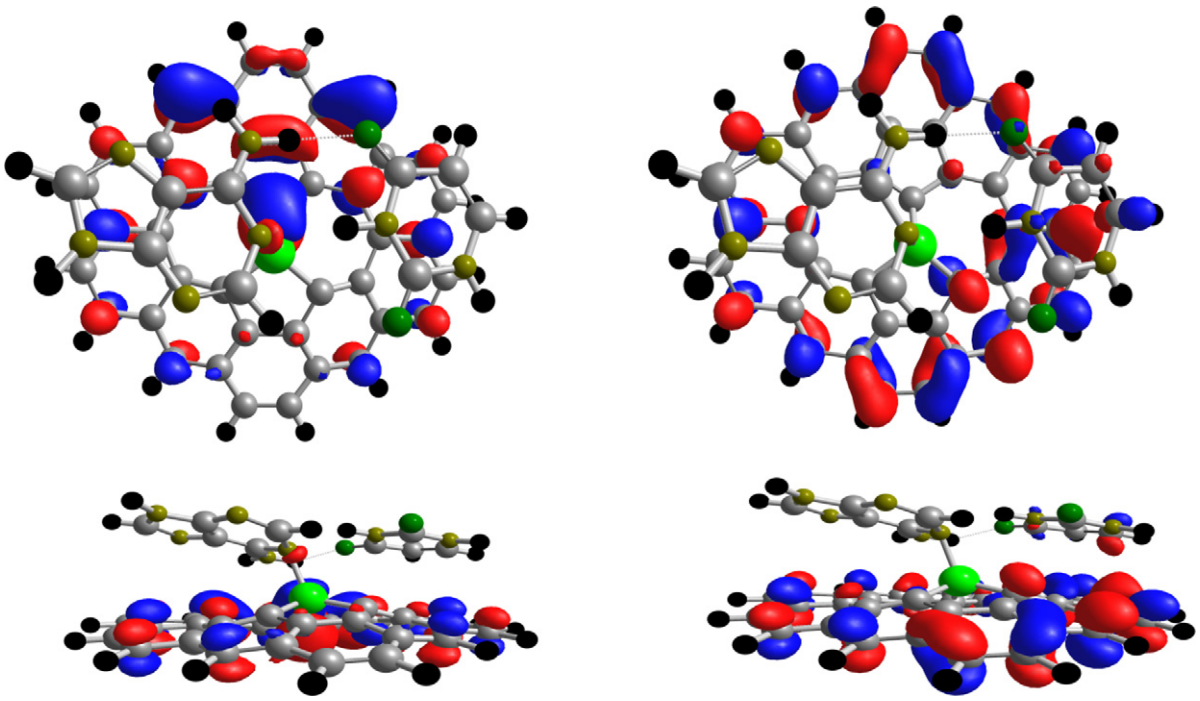

c) AU-Si-SW

Fig. 5 (*continued*).

The N_3-H_3···N_1 and N_6-H_6···O_4 H-bonds in both A-T and A-U base pairs, the N_3-H_3···N_1 bond is having smaller bond distance. This smaller bond distance leads to higher $\rho(r_c)$ (0.041 a.u) and stabilization energy (E^2) of N_3-H_3···N_1 bond (28.24 kcal/mol for A-U and 27.81 kcal/mol for A-T base pair) than the N_6-H_6···O_4 bond calculated by topological and NBO analysis which are given in Table 7. Among A-T and A-U, A-U base pair has slightly higher interaction (−16.38 kcal/mol) energy [57] than the A-T (−16.24 kcal/mol) base pair, due to their smaller H-bond distance between donor and acceptor region. Jens Antony et al. [47] also reported that the A-U base pair has higher interaction energy (−17.9 kcal/mol) than the A-T (−17.7 kcal/mol) base pair, this result is well correlated with our present study. In the G-C base pair, the N_1 position of hydrogen (H_1) atom in the guanine residue interacted with N_3 position of cytosine residue. The amino group of H_2 atom in guanine residue is bonded with carbonyl group of O_2 atom in cytosine and vice-versa. In the G-C base pair, N_1-H_1··· N_3, N_2-H_2··· O_2, and N_4-H_4···O_6 bond distances are found to be 1.911 Å, 1.901 Å, and 1.779 Å. Among A-T, G-C and A-U base pair, the G-C base pair is the most stable structure because G-C structure is stabilized by three H-bond interactions and it has higher interaction energy (−31.87 kcal/mol) than A-T and A-U base pair. The interaction energy order of isolated base pair is found to be G-C > A-U > and A-T [57].

Further, DNA/RNA base pairs are stacking with defective and defect-dopant graphene sheets through π-π stacking interaction. Initially, DNA/RNA base pairs with defective and defect-dopant graphene sheets are kept at a distance of ~3 Å, and geometry optimizations are done to obtain the minimum energy structures. The optimized structures are shown in Figs. 4, and Supplementary Figure (S1, and S2) their corresponding bond distance and angles are given in Tables 2–4. During complex formation, the N_3-H_3···N_1 (A-T & A-U) H-bond is contracted and elongated around 0.012–0.016 Å (A-T) and 0.021–0.023 Å (A-U), similarly N_6-H_6···O_4 bond distance is contracted and elongated around 0.009–0.012 Å (A-T) and 0.019–0.021 Å (A-U), whereas their corresponding bond angles are contracted and elongated around 2–7° in DV, B-DV, Si-DV, SW, and B-SW graphene sheet. In G-C base pair, the N_1-H_1···N_3, N_2-H_2···O_2, and N_4-H_4···O_6 bond distance variations are found to be 0.016–0.018 Å (N_1-H_1···N_3), 0.027–0.044 Å (N_2-H_2···O_2), and 0.027–0.037 Å (N_4-H_4···O_6) in DV, B-DV, Si-DV, SW, and B-SW graphene sheet. But in the case of DNA/RNA base pair on Si-SW graphene sheet, the H-bonds are highly distorted around 0.294 Å (A-T), 0.372 Å (G-C), and 0.276 Å (A-U). Because Si atom in SW sheet is strongly interacted with the nitrogen (N_1) atom of adenine base in both A-T and A-U base pair, as well N_3 atom of cytosine base in G-C base pair, due to higher electrophilic nature of N_1/N_3 atom bonded with higher nucleophilic nature (1.67 eV) of Si atom [36]. Their corresponding bond distance of Si—N is found to be 1.94 Å and this result in good agreement with previous result [51]. The calculated vertical rise between the DNA/RNA base pair and DV, B-DV, Si-DV, SW, and B-SW are varied from 3 to 3.5 Å, the shortest distance are observed at 1.94 Å, 1.93 Å, and 1.95 Å for A-T, G-C, and A-U in Si-SW. These large structural distortion leads to decreasing H-bond energy while compared with isolated DNA/RNA base pair, the calculated H-bond energy between base pairs in DV, B-DV, Si-DV, SW, B-SW, and Si-SW are given in Table 6a. In addition to that the total adsorption energies are calculated for each fragment in complex structure with counterpoise method. Among A-T, G-C, and A-U base pair with defective and defect-dopant graphene sheet, the G-C (−78.8 kcal/mol) base pair shows the highest interaction energy than A-T and A-U, these result is related with the previous experimental [58] and theoretical result [57]. Additionally, the nature of interactions between Si and N_1 atom is investigated using topological analysis and these findings confirmed that the partial electrostatic and partial covalent interactions (Si···N_1/N_3) are obtained during complexation [36]. This kind of interaction (partial electrostatic and partial covalent interaction) is the main reason for the highest adsorption energy to obtain during complex formation between DNA/RNA base pair and Si doped SW sheet. Further, the electronic properties and charge transfer mechanism are also found for DNA/RNA base pair into defective and defect-dopant graphene sheet using DOS, FMO, and EDDM analysis.

3.2. Adsorption energy

The adsorption energies are calculated for isolated DNA/RNA base pair and DNA/RNA base pair stacking on defective and defect-dopant graphene sheet with BSSE correction using wB97XD and M06-2X level of theories and their values are given in Table 6a. The H-bond energy of isolated DNA/RNA base pair is obtained at −16.24 kcal/mol for A-T, −31.87 kcal/mol for G-C, and −16.38 kcal/mol for A-U. Among A-T, G-C and A-U, the G-C base pair has the highest adsorption energy than other base pair. The presence of strong three H-bond interaction leads to the highest interaction energy of G-C pair and these results in good agreement with previous result [59,60]. The H-bond energy of the isolated DNA/RNA base pair order is in the following order G-C > A-U > A-T [57]. The H-bond energies of DNA/RNA base pair in the presence DV sheet are found to be −15.89 kcal/mol (A-T), −31.30 kcal/mol (G-C), and −15.91 kcal/mol (A-U). In B-DV and Si-DV sheet, the H-bond energies are observed at −16.06 kcal/mol & −16.04 kcal/mol (A-T), −31.56 kcal/mol & −31.48 kcal/mol (G-C), and −16.09 kcal/mol & −16.18 kcal/mol (A-U). Similarly, DNA/RNA base pair on the SW and B-SW sheets are obtained at −15.82 kcal/mol & −16.01 kcal/mol (A-T), −31.72 kcal/mol & −31.52 kcal/mol (G-C), and −15.90 kcal/mol & −16.37 kcal/mol (A-U). In the case of DNA/RNA base pair on the Si-SW sheet is obtained at −9.12 kcal/mol, −27.32 kcal/mol, and −12.38 kcal/mol for A-T, G-C, and A-U base pairs. It can be observed that the H-bonding energies of DNA/RNA base pairs decrease in magnitude in the defective and defect-dopant graphene sheet while compared with the isolated base pair. This is because of the structural distortion occurred in the DNA/RNA base pairs when adsorbing with the defective and defect-dopant graphene sheet. Thus, the distortion energies are calculated for DNA/RNA base pairs in the defective and defect-dopant graphene sheet, their energy values are given in Table 5. The distortion energy variations are found to be −0.18 kcal/mol to −0.42 kcal/mol for A-T, −0.15 kcal/mol to −0.57 kcal/mol for G-C, and −0.2 kcal/mol to −0.48 kcal/mol for A-U base pair in the DV, B-DV, and Si-DV sheet. In SW and B-SW sheet, the distortion energy variations are obtained at −0.42 kcal/mol & −0.23 kcal/mol for A-T, −0.15 kcal/mol & −0.35 kcal/mol, and −0.01 kcal/mol to −0.48 kcal/mol for A-U base pair. But in the case of Si-SW sheet, the distortion energy is found to be

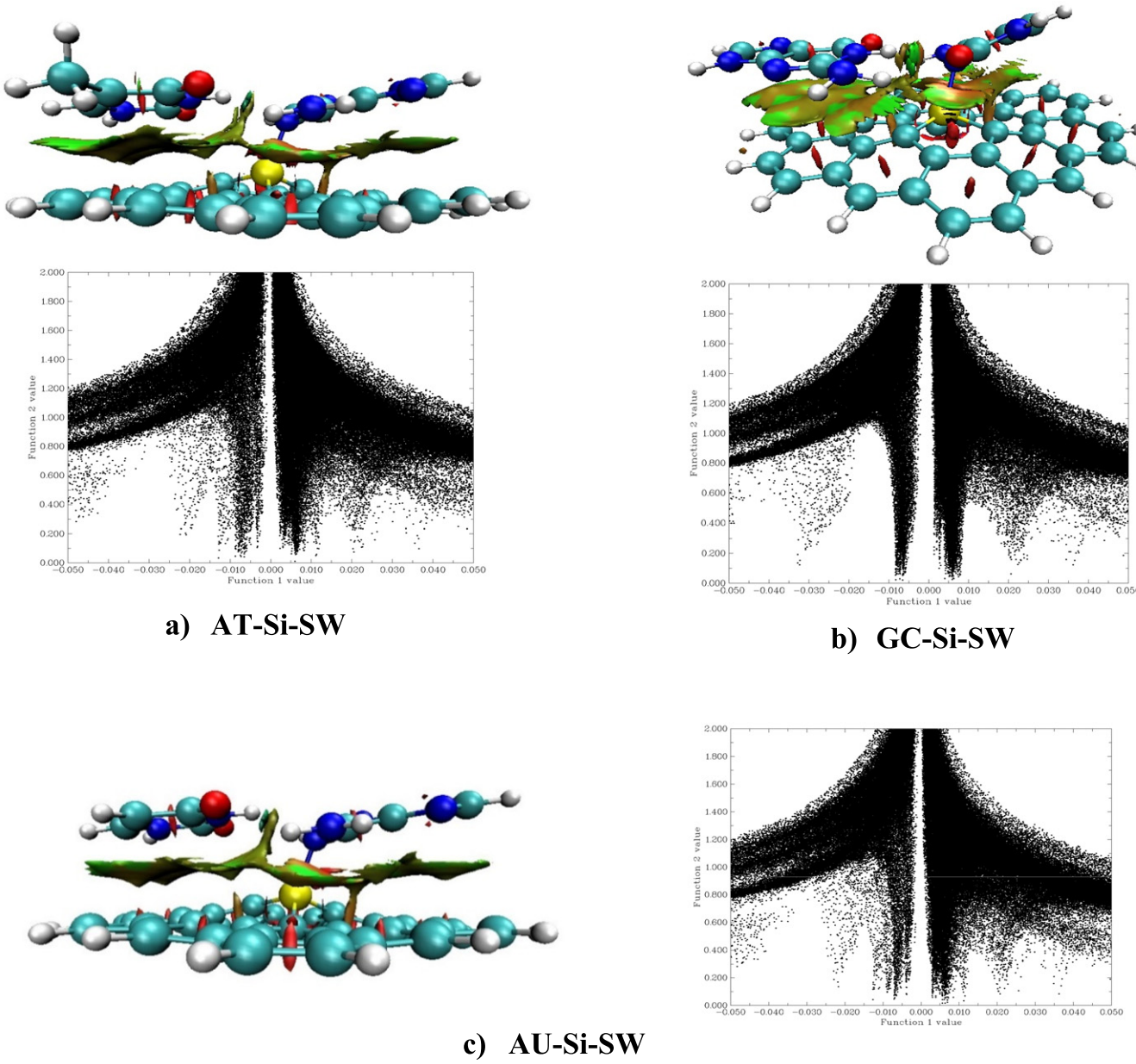

Fig. 6. Non-covalent interaction plot for DNA/RNA base pairs on Si-SW defective sheets are calculated using M06-2X level of theory.

−7.12 kcal/mol for A-T, −4.55 kcal/mol for G-C, and −4.00 kcal/mol for A-U base pair. The largest structural distortion is arisen between DNA/RNA base pair and Si-SW sheet because of the strong interaction between Si and N which is decreasing the H-boding between base pair [59]. The decreasing H-bond interaction between base pair to obtain lower interaction energy (−9.12 kcal/mol (A-T), −27.32 kcal/mol (G-C), and −9.22 kcal/mol (A-U)) and their electron density values are decreased around 0.002–0.04 a.u (see Table S4). The corresponding NPA atomic charges of N_1/N_3 atom in DNA/RNA base pair also decreases from −0.365 eV to −0.293 eV (A-T), −0.395 eV to −0.146 eV (G-C), and −0.350 eV to −0.299 eV (A-U). The Mulliken atomic charges are also given in the Table S3. The decreasing H-bond between DNA/RNA base pair is mainly due to the decreasing electron density as well as atomic charges between DNA/RNA base pair which obtained the lower H-bond energy on Si-SW sheet. The strength of the H-bond energies of base pair with the defective and defect-dopant sheet follow the order G-C > A-T > A-U.

Further, the total adsorption energies are calculated for the complex structure at the same level of theory using two and three fragmentation method, the calculated fragment energy values are given in Table 6a and comparison adsorption values are given in Table 6b. The procedure to calculate the total energy of the complex system has conversed in the computational details. DNA nucleobases (A, T, G, and C) on defective and defect-dopant graphene sheets are compared with previous carbon based materials, gold nanoparticles (AuNPs) and Au(111) surface. N. Varghese et al. [58] reported that the adsorption energy of graphene with DNA nucleobases and base pairs were −11.85 kcal/mol (A), −4.72 kcal/mol (T), −13.45 kcal/mol (G), −9.38 kcal/mol (C), −9.73 kcal/mol (AT), and −12.3 kcal/mol (GC). The adsorption energy of nucleobases on graphite C(0001) is −1.2 kcal/mol (A), −7.65 ± 0.7 kcal/mol (T), −12.67 ± 2.6 kcal/mol (G), and −7.89 ± 1.9 kcal/mol (C), similarly adsorption energy of nucleobases on Au(111) surface is −8.60 ± 2.6 kcal/mol (A), −5.02 ± 1.7 kcal/mol (T), −6.93 ± 0.7 kcal/mol (G), and −6.69 ± 0.5 kcal/mol (C) reported by Hughes, Z et al. [61]. Das et al. [62] also found the adsorption energy of nucleobases on SWNT is −0.22 kcal/mol (A), −0.32 kcal/mol (T), and −0.13 kcal/mol (C). A. Gourishankar et al. [63] has reported that the adsorption energy of DNA bases with AuNPs using isothermal titration calorimetry studies (ITC), the corresponding values are −0.25 kcal/mol (A), −0.43 kcal/mol (G), and −0.73 kcal/mol (C). The obtained results are well correlated with previous experimental [58,61] and theoretical [38,51,64] value. In the present work, DNA/RNA base pair on DV, B and Si doped DV sheet, the adsorption energies are found to be in the range of −13.25 to −19.03 kcal/mol (DV), −12.71 to −19.27 kcal/mol (B-DV) and −12.92 to −16.35 kcal/mol (Si-SW). Similarly, the adsorption value of SW, B-SW, and Si-SW sheet with DNA/RNA base pairs are found to be in the rage of −9.83 to −16.21 kcal/mol (SW), −12.35 to −16.45 kcal/mol, (B-SW) and −9.39 kcal/mol to −49.18 kcal/mol (Si-SW). While comparing these previous experimental results, DNA nucleobases on defective and defect-dopant graphene sheet have higher adsorption energy. Among DV, B-DV, Si-DV, SW, B-SW, and Si-SW, the Si-SW has higher adsorption energy and this result is strongly concluding that the Si-SW sheet can be a better sensing material for DNA nucleobases. Then the adsorption energies of DNA/RNA base pairs on defective and defect-dopant graphene sheets are exposed that among all the DNA/RNA base pairs, the G-C base pair has the highest adsorption energy with the entire defective and defect-dopant graphene sheet. Previous reports on DNA/RNA base pair on graphene complexes have also shown the highest adsorption energies for G-C base pair [47]. G-C base pair has been obtained to exhibit the highest adsorption energies for adsorption on numerous other substrates like graphyne [59], graphdiyne [57] and BN sheet [65]. According to Table 6a, DNA/RNA base pair on DV sheet is found to be −44.17 kcal/

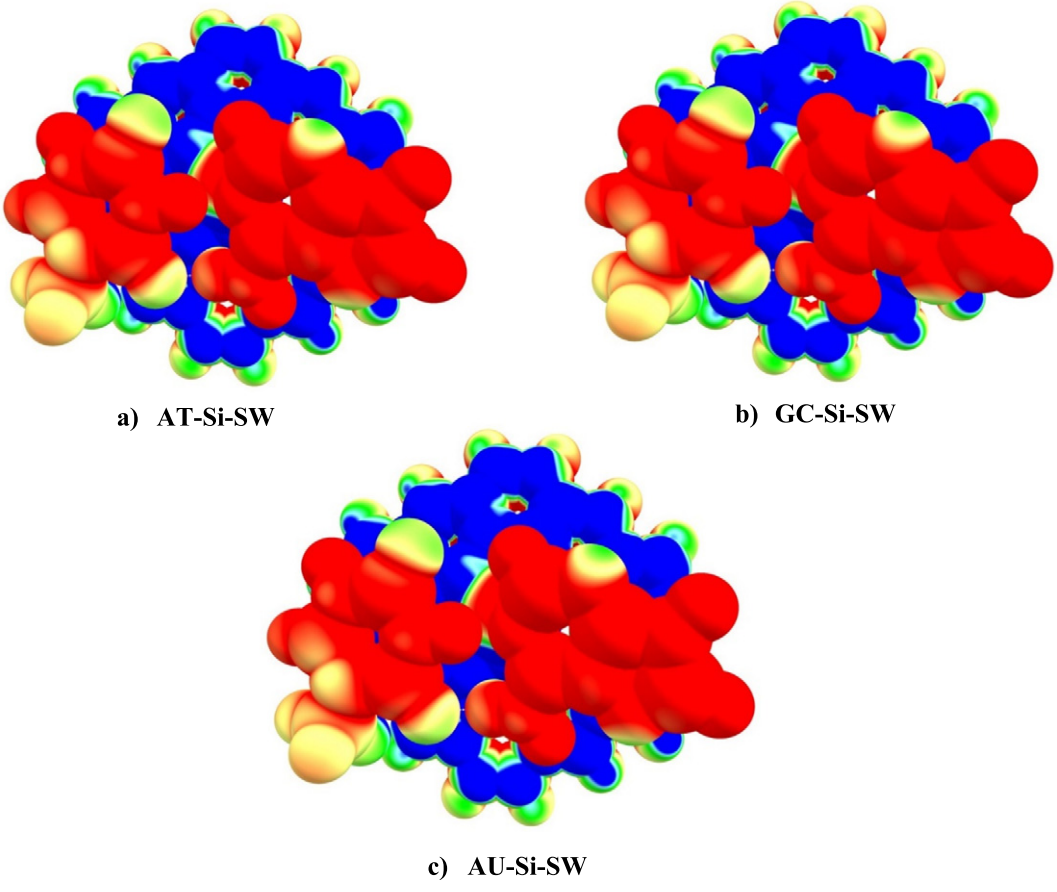

Fig. 7. Charge transfer mechanism calculated for DNA/RNA base pair on Si-SW defective sheet is calculated using EDDM analysis by M06-2X level of theory.

mol for A-T, −61.51 kcal/mol for G-C and −44.67 kcal/mol for A-U. Similarly, in B-DV sheet is observed at −43.09 kcal/mol for A-T, −61.40 kcal/mol for G-C and −45.10 kcal/mol for A-U base pair. From the result, A-U base pair adsorbs strongly over B-DV graphene than the DV sheet. In Si doped DV sheet, the adsorption energies are obtained at −43.49 kcal/mol for A-T, −62.32 kcal/mol, and −43.59 kcal/mol for A-U base pair. The order of adsorption energy is found to be in the sheet Si-DV > B-DV > DV.

It can be clearly shown that the adsorption energies of B-DV and Si-DV sheets are high towards DNA/RNA base pair than the bare DV sheet. Thus, the presence of B and Si atom increase the conductivity of DV sheet and it enhances the adsorption energy [28,60]. The similar trend is also found for the DNA/RNA base pair on SW, B-SW, and Si-SW sheet. The adsorption energies in SW and B-SW sheets are -41.82 kcal/mol & -41.12 kcal/mol for A-T, -59.02 kcal/mol & -60.23 kcal/mol for G-C, and -40.56 kcal/mol & -40.79 for A-U. In B-SW sheet, the adsorption energies are increased around 1-2 kcal/mol than the bare SW sheet. But the Si atom is doped with SW sheet, the adsorption energies are drastically increased around 20-25 kcal/mol. The total adsorption energy of the Si doped SW complex system is found to be -70.21 kcal/mol for A-T, -80.59 kcal/mol for G-C, and -69.78 kcal/mol for A-U complex. This is because the presence of Si atom in SW sheet highly interacts with cytosine base in G-C, similarly adenine base in A-T and A-U base pair due to the strong interaction between Si and N atom. The order of total adsorption energies in SW, B-SW and Si-SW sheets are Si-SW > B-SW > SW.

In some complex structure, the difference between two and three fragment values are obtained to be positive around 0.2-4.4 kcal/mol which is pairwise adsorptions, slightly weakened in the triad [59]. The obtained results clearly exposed that G-C base pair has the highest interaction energy on Si doped SW and DV sheets and these results are good agreement with previous result [51]. Previous experimental [58] and theoretical results [47] have also found that G-C base pair has the highest adsorption energy towards graphene material. Moreover, the highest adsorption energy of the G-C base pair on layered materials agrees with the isothermal titration calorimetry experiments advanced for DNA base pair with graphene complexes [58]. The adsorption energy of the sheet follows the order Si-SW > Si-DV > B-DV > DV> B-SW > SW and this result is well correlated with topological analysis.

3.3. Topological analysis

The QTAIM is used to explore the interaction between the DNA/RNA base pair and defective and defect-dopant graphene sheets. The $\rho(r)$ and $\nabla^2\rho(r)$ at the bond critical point (BCP) is used to define the bonding strength. The H(r) is used to understand the nature of the interaction (whether covalent or electrostatic) between two atoms [66]. If

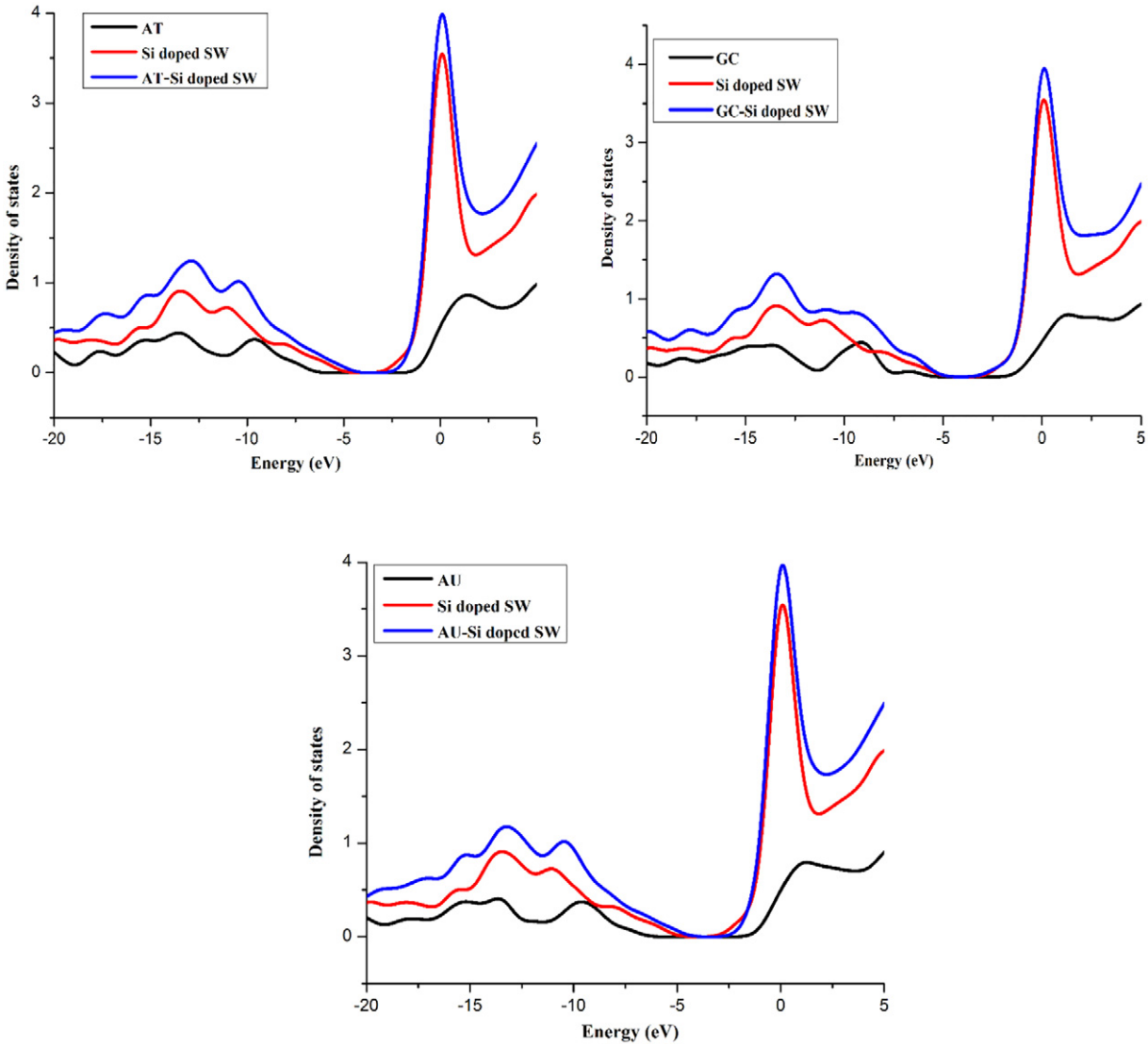

Fig. 8. The density of states for DNA/RNA base pairs on Si-SW defective sheets are calculated by M06-2X level of theory.

the value of H(r) is positive, then the interaction is electrostatic nature; otherwise the interaction is covalent nature. A negative value of $\nabla^2\rho(r)$ represents the covalent bond interaction, whereas a positive value indicates the closed-shell interaction (electrostatic interaction, H-bond, and π-π stacking interaction). The $\rho(r)$ value is the order of 0.1 a.u for covalent bond interaction, while in the case of electrostatic interaction, the $\rho(r)$ value is 0.01 a.u or even less [51]. Herein, the nature of interaction between Si and N atom is investigated by H(r), $\nabla^2\rho(r)$, and $\rho(r)$ parameter. The calculated $\rho(r)$, $\nabla^2\rho(r)$ and (H(r)) values of Si-SW sheet with A-T, G-C and A-U are given in Table 7. According to Table 7, the $\rho(r)$ values between N_1/N_3 and Si are observed at 0.079 a.u for A-T, 0.076 a.u for G-C, and 0.079 a.u for A-U. The corresponding $\nabla^2\rho(r)$ and H(r) values are found to be 0.250 a.u & -0.031 a.u for A-T, 0.030 a.u & -0.020 a.u for G-C, and 0.244 a.u & -0.031 a.u for A-U. The obtained $\rho(r)$ values between Si and N in both A-T/A-U and G-C on Si doped SW sheet is lying between electrostatic and covalent interactions. Further, a positive $\nabla^2\rho(r_c)$ and negative H(r) signature indicate that the interaction between Si and N (Si···N) is partially electrostatic and partially covalent interaction [36]. Thus, the formation of intermolecular interaction between base pair and Si-SW sheet is governed by both Si···N and π-π stacking interaction and these interactions are main responsible to obtain the highest interaction energy which is in close agreement with the previous theoretical study [36]. Further, the role of electrostatic interaction to the physisorption stability for the defective and defect-dopant complex structures are also addressed by using the $\rho(r)$ at the BCPs of intermolecular interactions are investigated, which is at the BCPs in intermolecular bond paths connecting the nuclear critical points (NCPs) and are given in Table S4. Table S4 displays that the magnitude of the intermolecular electrostatic interactions is higher for Si-SW (≈0.008 a.u to 0.012 a.u) and DV (≈0.007 a.u to 0.007 a.u) sheets than the other defect and doped sheet. The higher electrostatic interaction has occurred between the pyramidal ring of base pair and π-centre of the Si doped heptagon-pentagon ring of the SW sheet due to the high charge transfer between base pair and sheet. The high $\rho(r)$ value leads to the higher interaction energy between DNA/RNA base pair and Si-SW sheet, the stability is found in the order of Si-SW > Si-DV > DV > B-DV> B-SW > SW and this result is well correlated with our adsorption energy analysis. Further, the aromatic character is investigated for the pyrimidine and imidazole rings of base pairs by MCBO index [67] which depends on electron delocalization properties [68] before and after adsorption of base pair on defective and defect-

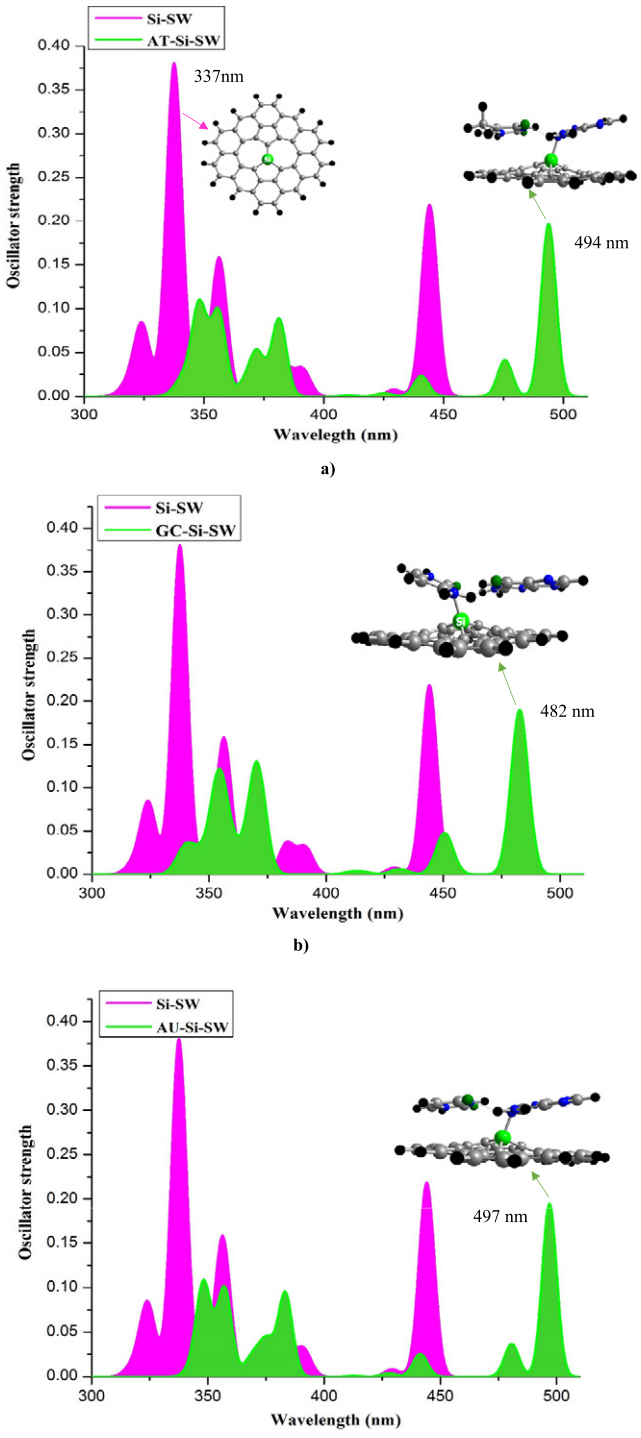

Fig. 9. Absorption spectra for DNA/RNA base pairs on Si-SW defective sheets are calculated using TD-DFT method by M06-2X level of theory.

Table 2
Bond distance and bond angles are calculated for base pair in DV and SW sheets using M06-2X with 6-311+g* level of theory.

Base pairs in complex	DV sheet		SW sheet	
	Bond distance (Å)	Bond angle (°)	Bond distance (Å)	Bond angle (°)
AT				
N_3-H_3···N_1	1.806	171.8	1.785	177.9
N_6-H_6···O_4	1.963	173.9	1.909	170.2
GC				
N_1-H_1··· N_3	1.919	174.0	1.909	174.7
N_2-H_2··· O_2	1.897	179.0	1.872	173.4
N_4-H_4···O_6	1.819	175.6	1.822	175.3
AU				
N_3-H_3···N_1	1.790	169.1	1.822	178.5
N_6-H_6···O_4	1.975	172.1	1.925	171.3

Table 3
Bond distance and bond angles are calculated for base pair in B doped DV and SW sheets using M06-2X with 6-311+g* level of theory.

Base pairs in complex	B doped DV sheet		B doped SW sheet	
	Bond distance (Å)	Bond angle (°)	Bond distance (Å)	Bond angle (°)
AT				
N_3-H_3···N_1	1.785	177.5	1.797	177.2
N_6-H_6···O_4	1.956	172.0	1.986	170.4
GC				
N_1-H_1···N_3	1.910	174.5	1.911	174.0
N_2-H_2···O_2	1.888	179.3	1.885	171.8
N_4-H_4···O_6	1.814	176.4	1.835	173.8
AU				
N_3-H_3···N_1	1.838	175.6	1.793	178.4
N_6-H_6···O_4	1.917	173.3	1.925	170.7

dopant graphene sheets. The MCBO index of pyrimidine and imidazole rings are portrayed in Fig. S10. From Figure shows S10, the higher the MCBO indicates, the higher the strength of the multicenter bond (aromaticity). The decreasing aromatic character of the DNA/RNA base is found in the order of A > G > C > T > U and this quite favors with previous result [57]. The MCBO value of pyrimidine and imidazole rings of isolated base is obtained at 0.50 a.u-0.60 a.u and 0.50-0.52 a.u; when the π-π stacking takes place on defective and defect-dopant graphene sheets, the MCBO index is changed around 0.05-0.07 a.u (SW & doped SW) and 0.05-0.1 a.u. Hence, the MCBO index revealed that the aromatic character of the base pair is almost not affected by the SW and doped SW graphene sheets.

In addition, the non-covalent interaction (NCI) analysis [69] is done to get insights into the qualitative decoration of the weak interactions between the molecules governing the physisorption. The NCI analysis depends on the reduced density gradient s and electron density (ρ) is given by

$$S = \nabla\rho / \left(2\left(3\pi^2\right)^{1/3}\rho^{4/3}\right).$$

This sign is related to the long-range interactions at low ρ regions; the low ρ region relates to the sign of the λ_2 (second largest Eigenvalue of the Hessian matrix of the electron density). The weak vdW (van der Waals) interactions are found at $\lambda_2 \approx 0$; whereas, the H-bonds and steric repulsive interactions have occurred at $\lambda_2 < 0$ and $\lambda_2 > 0$. The NCI analysis for DNA/RNA base pair on Si-SW sheet is depicted in Fig. 6 (3D NCI plot). In the 3D NCI map, blue colour represents H-bond interaction, green colour indicates vdW interaction and red colour point out the strong repulsion (steric effect) between molecules. In Figure S6, the blue colour is observed at N_3-H_3···N_1, N_6-H_6···O_4 (A-T & A-U), N_1-H_1··· N_3, N_2-H_2··· O_2, and N_4-H_4···O_6 in G-C base pair, the corresponding peaks are obtained at ≈-0.025 a.u and ≈-0.050 a.u at the negative region. The vdW interactions regions have occurred from ≈-0.015 a.u to ≈0.010 a.u, and the strong repulsion region is observed in benzene ring at ≈0.025 a.u for both DV and SW sheet. While in the case of B-DV, B-SW and Si-DV sheet, the H-bond peaks are obtained at ≈-0.025 a.u and ≈-0.045 a.u. From the obtained result revealed that there is no large structural deviation are pronounced during intermolecular complex formation. Due to the strong interaction between Si and N, the magnitude of H-bond interaction is reduced in DNA/RNA on Si-SW sheet. The H-bond peaks have appeared at ≈0.005 a.u near vdW region which is clearly shown in Figure S7. The strong repulsion region has appeared in the positive region around ≈0.020 to 0-040 a.u, a positive λ_2 values pronounced the steric interaction acted between DNA/RNA base pair Si-SW sheet, this is due to the main contribution of π-orbitals of DNA/RNA base pair too close in the substrate [70]. Fascinatingly the 3D plots show a similar pattern where green and red colour shows that the vdW interactions and steric interactions between molecules. Their corresponding electron density values are decreased 0.021 a.u & 0.023 a.u for A-T, 0.014 a.u, 0.012 a.u, and 0.025 a.u for G-C and 0.022 a.u & 0.024 a.u for A-U complex. The reducing electron density values exposed that the large structural distortion occurred during complexation between DNA/RNA base pair and Si-SW sheet, this result is good agreement with our adsorption and distortion energy analysis. From the obtained topological results concluded that the DNA/RNA base pair is highly adsorbed on Si doped SW sheet than the other sheets; the interactive nature of Si···N bond is partially electrostatic and partially covalent nature.

3.4. Electronic properties of DNA/RNA on defect and defect-dopant graphene sheet

The NPA charge analysis is calculated for DNA/RNA base pair on a defective and defect-dopant graphene sheet. After the adsorption of DNA/RNA base pair on defective and defect-dopant graphene sheet, the NPA charge of DNA/RNA base pair is decreased around -0.21 eV for A-T (at N_1), -0.4 eV (at N_3) for G-C, and -0.23 eV (N_1) for A-U on DV sheet (see Table S2 and S3). In B-DV and Si-DV sheet, the positive values are obtained at A-T (N_1), G-C (N_3), and A-U (N_1) base pair which specifies that the charge is transferred from DNA/RNA base pair to B-DV and Si-DV sheet [51]. DNA/RNA base pair on SW, B-SW and Si-SW sheet, the NPA charge variation decreasing around -0.12 to -0.35 eV (SW) and -0.22 to -0.40 eV (B-SW & Si-SW). These values indicated that the charge transfer takes place from DNA/RNA base pair to defect and defect-dopant graphene sheet [36] and further which is confirmed by EDDM map analysis. The isosurface of EDDM is calculated by subtracting the electron density of isolated base pairs and defect-dopant sheets from that of their complex structures. The calculated EDDM for the complex of DNA/RNA base pairs and Si-SW sheets are shown in Fig. 7. In Fig. 7, blue colour represents the electron density increases and red colour represents electron density decreases. It can be clearly shown that the electron density rich region occurs in Si-SW sheet and the electron density depletion region occurs in G-C, A-T and A-U base pair. These obtained results exposed that the charge transfer change from N_1/N_3 to Si atom in SW sheet which is further confirmed by FMO analysis which is given in Fig. 5 and remaining structures are given in Figs. S3-S9. It must be important to note that the charge transfer mechanism is the main reason for the changes in the conductivity of the defective sheet by doping and it enhances the sensing properties as well as adsorption energy towards DNA/RNA constituents. Further, the change in electronic properties of DNA/RNA base pairs adsorbed on defect-dopant sheets is calculated by ΔE_{HL} and DOS analysis which is given in Figs. 8 and S16. The ΔE_{HL} values for complex structure are listed in Table 8. It can be observed that both ΔE_{HL} gap and DOS do not modify upon the adsorption of DNA/RNA base pairs on DV, B-DV, Si-DV, SW, and B-SW. On the other hand, the significant changes are observed in the DNA/RNA base pair on Si-SW. The ΔE_{HL} gap is reduced around 0.1 eV for A-T, 0.3 eV for G-C, and 0.2 eV for A-U. The ΔE_{HL} gap of isolated DNA/RNA base pair and bare Si-SW sheet is obtained at 7.1 eV (A-T),

Table 4
Bond distance and bond angles are calculated for base pair in Si doped DV and SW sheets using M06-2X with 6-311+g* level of theory.

Base pairs in complex	Si doped DV sheet		Si doped SW sheet	
	Bond distance (Å)	Bond angle (°)	Bond distance (Å)	Bond angle (°)
AT				
N_3-H_3···N_1	1.784	177.0	2.112	152.1
N_6-H_6···O_4	1.926	173.4	1.977	145.1
GC				
N_1-H_1···N_3	1.919	176.4	2.299	174.7
N_2-H_2···O_2	1.888	176.3	1.871	173.7
N_4-H_4···O_6	1.837	175.7	1.834	175.
AU				
N_3-H_3···N_1	1.769	179.3	2.089	–
N_6-H_6···O_4	1.928	172.3	1.956	149.2

Table 5
Distortion energies of the DNA/RNA base pairs into the defected and defect-dopant graphene sheet employing M06-2X/wB97XD level of theories.

Complex	Distortion energy (kcal/mol)					
	A-T		G-C		A-U	
	M06-2X	wB97XD	M06-2X	wB97XD	M06-2X	wB97XD
DV	−0.30	−0.35	−0.41	−0.57	−0.06	−0.47
B-DV	−0.14	−0.18	−0.32	−0.23	−0.31	−0.29
Si-DV	−0.25	−0.20	−0.34	−0.39	−0.16	−0.20
SW	−0.31	−0.42	−0.35	−0.15	−0.50	−0.48
B-SW	−0.13	−0.23	−0.44	−0.35	−0.03	−0.01
Si-SW	−4.32	−7.12	−6.70	−4.55	−3.98	−4.00

7.0 eV (A-U), 6.1 eV (G-C) and 4.0 eV (Si-SW). After the complex formation, the ΔE_{HL} gap is reduced at 3.9 eV (AT-Si-SW), 3.7 eV (GC-Si-SW), and 3.8 eV (AU-Si-SW) respectively and these remarks are in good agreement with DOS analysis. The reduction of ΔE_{HL} increase the number of electrons in the conduction band, thus it increases the conductivity of the sheet. The ΔE_{HL} and DOS results confirmed that DNA/RNA base pair change the electronic structure of Si-SW sheet during adsorption process. These electronic changes are enhancing the conductivity behaviour of Si-SW sheet [34]. From the obtained results, the Si-SW sheet is favourable for the chemical sensing of DNA/RNA

Table 6a
The total adsorption energies are calculated for A-T, G-C, and A-U base pair on DV, B doped DV, Si doped DV, SW, B doped SW, and Si doped SW using M06-2X and wB97XD level of theory with BSSE correction.

Adsorption energy (kcal/mol)						
Complex	M06-2X	wB97XD	Available literature value	Complex	M06-2X	wB97XD
AT-DV				**AT-SW**		
$\Delta^2E_{(iso)}$	−15.04	−16.24		$\Delta^2E_{(iso)}$	−15.04	−16.24
$\Delta E_{(Tot)}$	−38.64	−44.17	[−17.7][a]	$\Delta E_{(Tot)}$	−35.79	−41.82
$\Delta E_{(A-T)}$	−14.74	−15.89		$\Delta E_{(A-T)}$	−14.73	−15.82
$\Delta E_{(A+DV)}$	−12.17	−14.90	[−15.1][b]	$\Delta E_{(A+DV)}$	−13.18	−16.03
$\Delta E_{(T+DV)}$	−11.88	−13.71	[−15.8][b]	$\Delta E_{(T+DV)}$	−7.81	−9.83
Δ^3E	0.15	0.33		Δ^3E	−0.07	−0.14
GC-DV				**GC-SW**		
$\Delta^2E_{(iso)}$	−30.33	−31.87	[−32.3][a]	$\Delta^2E_{(iso)}$	−30.33	−31.87
$\Delta E_{(Tot)}$	−56.10	−61.51		$\Delta E_{(Tot)}$	−51.99	−59.02
$\Delta E_{(G-C)}$	−29.92	−31.30		$\Delta E_{(G-C)}$	−29.98	−31.72
$\Delta E_{(G+DV)}$	−16.95	−19.03	[18.0][b]	$\Delta E_{(G+SW)}$	−11.26	−15.50
$\Delta E_{(C+DV)}$	−11.15	−13.25	[11.6][b]	$\Delta E_{(C+SW)}$	−12.98	−16.21
Δ^3E	1.92	2.07		Δ^3E	2.23	4.41
AU-DV				**AU-SW**		
$\Delta^2E_{(iso)}$	−15.24	−16.38	[−17.9][a]	$\Delta^2E_{(iso)}$	−15.24	−16.38
$\Delta E_{(Tot)}$	−38.39	−44.67		$\Delta E_{(Tot)}$	−34.66	−40.56
$\Delta E_{(A-U)}$	−15.18	−15.91		$\Delta E_{(A-U)}$	−14.74	−15.90
$\Delta E_{(A+DV)}$	−12.51	−16.93		$\Delta E_{(A+SW)}$	−10.24	−12.67
$\Delta E_{(U+DV)}$	−11.39	−12.16	[15.1][b]	$\Delta E_{(U+SW)}$	−9.65	−11.98
Δ^3E	0.69	0.33		Δ^3E	−0.03	−0.01
AT-B-DV				**AT-B-SW**		
$\Delta^2E_{(iso)}$	−15.04	−16.24	–	$\Delta^2E_{(iso)}$	−15.04	−16.24
$\Delta E_{(Tot)}$	−37.73	−43.09		$\Delta E_{(Tot)}$	−36.15	−41.12
$\Delta E_{(A-T)}$	−14.89	−16.06		$\Delta E_{(A-T)}$	−14.91	−16.01
$\Delta E_{(A+B-DV)}$	−12.47	−14.98		$\Delta E_{(A+SW)}$	−10.62	−13.06
$\Delta E_{(T+B-DV)}$	−10.62	−12.35		$\Delta E_{(T+SW)}$	−10.96	−12.35
Δ^3E	0.25	0.3		Δ^3E	0.34	0.3
GC-B-DV				**GC-B-SW**		
$\Delta^2E_{(iso)}$	−30.33	−31.87	–	$\Delta^2E_{(iso)}$	−30.33	−31.87
$\Delta E_{(Tot)}$	−56.01	−61.40		$\Delta E_{(Tot)}$	−53.77	−60.23
$\Delta E_{(G-C)}$	−30.01	−31.56		$\Delta E_{(G-C)}$	−29.89	−31.52
$\Delta E_{(G+B-DV)}$	−11.04	−12.71		$\Delta E_{(G+B-SW)}$	−12.07	−14.17
$\Delta E_{(C+B-DV)}$	−17.02	−19.27		$\Delta E_{(C+B-SW)}$	−14.11	−16.45
Δ^3E	2.08	2.14		Δ^3E	2.3	1.91
AU-B-DV				**AU-B-SW**		
$\Delta^2E_{(iso)}$	−15.24	−16.38	–	$\Delta^2E_{(iso)}$	−15.24	−16.38
$\Delta E_{(Tot)}$	−39.99	−45.10		$\Delta E_{(Tot)}$	−34.66	−40.79
$\Delta E_{(A-U)}$	−14.93	−16.09		$\Delta E_{(A-U)}$	−15.21	−16.37
$\Delta E_{(A+B-DV)}$	−10.68	−14.41		$\Delta E_{(A+B-SW)}$	−10.68	−14.26
$\Delta E_{(U+B-DV)}$	−10.23	−10.90		$\Delta E_{(U+B-SW)}$	−10.23	−11.38
Δ^3E	−4.15	−3.7		Δ^3E	1.46	1.22
AT-Si-DV				**AT-Si-SW**		
$\Delta^2E_{(iso)}$	−15.04	−16.24	–	$\Delta^2E_{(iso)}$	−15.04	−16.24
$\Delta E_{(Tot)}$	−38.85	−43.49		$\Delta E_{(Tot)}$	−59.12	−70.21
$\Delta E_{(A-T)}$	−14.79	−16.04		$\Delta E_{(A-T)}$	−10.72	−9.12
$\Delta E_{(A+B-DV)}$	−11.43	−12.92		$\Delta E_{(A+Si-SW)}$	−40.14	−49.18
$\Delta E_{(T+B-DV)}$	−13.03	−14.96		$\Delta E_{(T+Si-SW)}$	−8.90	−9.39
Δ^3E	0.4	0.43		Δ^3E	0.64	−2.52
GC-Si-DV				**GC-Si-SW**		
$\Delta^2E_{(iso)}$	−30.33	−31.87	–	$\Delta^2E_{(iso)}$	−30.33	−31.87
$\Delta E_{(Tot)}$	−57.97	−62.32		$\Delta E_{(Tot)}$	−78.76	−80.59
$\Delta E_{(G-C)}$	−29.99	−31.48		$\Delta E_{(G-C)}$	−23.63	−27.32
$\Delta E_{(G+Si-DV)}$	−12.95	−14.58		$\Delta E_{(G+Si-SW)}$	−10.90	−11.93
$\Delta E_{(C+Si-DV)}$	−14.98	−16.35		$\Delta E_{(C+Si-SW)}$	−50.61	−48.70
Δ^3E	0.04	0.09		Δ^3E	6.38	7.36
AU-Si-DV				**AU-Si-SW**		
$\Delta^2E_{(iso)}$	−15.24	−16.38	–	$\Delta^2E_{(iso)}$	−15.24	−16.38
$\Delta E_{(Tot)}$	−38.42	−43.59		$\Delta E_{(Tot)}$	−58.31	−69.78
$\Delta E_{(A-U)}$	−15.08	−16.18		$\Delta E_{(A-U)}$	−11.26	−12.38
$\Delta E_{(A+Si-DV)}$	−13.30	−14.96		$\Delta E_{(A+Si-SW)}$	−39.86	−48.24
$\Delta E_{(U+Si-DV)}$	−10.46	−12.78		$\Delta E_{(U+Si-SW)}$	−8.12	−9.22
Δ^3E	0.42	0.33		Δ^3E	0.93	0.06

[a] Ref. [47].
[b] Ref. [38].

Table 6b
Compare Adsorption energy between DNA/RNA base pairs interacted defective & defect dopant graphene sheet and other materials.

DNA with material	Adsorption energy (kcal/mol)	Available literature (kcal/mol)	
		Experimental	Theoretical
DV-A	−14.90	(−9.08 ± 1.2)[b]	(−15.1)[a]
DV-T	−13.71	(−7.65 ± 0.7)[b]	(−15.8)[a]
DV-G	−19.03	(−12.67 ± 2.6)[b]	(−18.8)[a]
DV-C	−13.25	(−7.89 ± 1.9)[b]	(−11.6)[a] (−10.61 to −16.34)[c]
B-DV-A	−14.98		
B-DV-T	−12.35	–	
B-DV-G	−12.71		(−10.15 to −16.37)[c]
B-DV-C	−19.27		
Si-DV-A	−12.92		(−38.01)[e]
Si-DV-T	−14.96	–	(−45.01)[e]
Si-DV-G	−14.58		(53.52)[e]
Si-DV-C	−16.35		(-34.41)[e]
SW-A	-16.03	(-11.85)[d]	(-17.75)[d]
SW-T	-9.83	(-4.72) [d]	(-16.63)[d]
SW-G	-15.50	(-13.45) [d]	(-19.10)[d]
SW-C	-16.21	(-9.38) [d]	(-14.52)[d]
B-SW-A	-13.06		
B-SW-T	-12.35	-	(10.15 to 16.37)[c]
B-SW-G	-14.17		
B-SW-C	-16.45		
Si-SW-A	-49.18		(-34.92)[e]
Si-SW-T	-9.39	-	(-30.90)[e]
Si-SW-G	-11.93		(-45.49)[e]
Si-SW-C	-48.70		(-50.90)[e]
SWNT-A	-	(-0.22)[f]	(-11.30)[f]
SWNT-T	-	(-0.32)[f]	(25.44)[g]
SWNT-G	-	-	(-11.76)[f] (7.63)[g]
SWNT-C	-	(-0.13)[f]	(-13.14)[f] (35.47)[g] (-6.92)[f] (35.74)[g]
AuNP-A	-	(-0.25)[h]	-
AuNP-T	-	-	-
AuNP-G	-	(-0.43)[h]	-
AuNP-C	-	(-0.73)[h]	-
Au(111)-A	-	(-8.60 ± 2.6)[i] (-22.13)[j]	(-8.4 ± 0.4)[i]
Au(111)-T	-		(-4.37 ± 0.1)[i]
Au(111)-G	-	(-5.02 ± 1.7)[i]	(-8.27 ± 0.3)[i]
Au(111)-C	-	(-6.93 ± 0.7)[i] (-6.69 ± 0.5)[i]	(-4.42 ± 0.2)[i]

[a] Ref [38].
[b] Ref [61].
[c] Ref [64].
[d] Ref [58].
[e] Ref [5].
[f] Ref [51].
[g] Ref [83].
[h] Ref [63].
[i] Ref [61].
[j] Ref [84].

constitutes and for the advance of new sensor or DNA/RNA sequencing devices [71–74].

3.5. Effect of the Optical properties

To comprehend the optical properties of bare defective and defect-dopant graphene sheet, isolated DNA/RNA base pair and their complex structures, the absorption spectra are evaluated using TD-DFT with the aid of M06-2X/6-311+g* level of theory. Previous experimental result [75] have found that the absorption region of DNA has occurred at 220 nm. Herein, the isolated A-T, G-C and A-U base pair, the maximum absorption peaks are calculated at 230 nm, 223 nm, and 231 nm, all these peaks correspond to n-π* transition [76]. The corresponding excitation energies are calculated at 5.280 eV for A-T, 5.557 eV for G-C, and 5.357 eV for A-U base pair, these results are in good agreement with previous reports [55,77].

Table 7
H bond and Si···N bond strengths are calculated for bare DNA/RNA base pair and base pair on Si doped SW sheet using topological analysis by M06-2X/6-311+g* level of theory.

Base pair	$\rho(r)$ in a.u	$\nabla^2\rho(r)$ in a.u	H(r) in a.u	$E^{(2)}$ kcal/mol
	Si-SW	Si-SW	Si-SW	
AT				
N_3-H_3···N_1	0.021 (0.024)[b]	0.076	0.002	27.81
N_6-H_6···O_4	0.023 (0.016)[b]	0.095	0.003	6.38
Si···N_1	0.079	0.250	-0.031 (-0.03)[a]	-
GC				
N_1-H_1··· N_3	0.014 (0.018) [b]	0.042	0.0005	18.62
N_2-H_2··· O_2	0.012 (0.022) [b]	0.040	0.0004	7.89
N_4-H_4···O_6	0.025 (0.023) [b]	0.096	0.002	11.97
Si···N_3	0.076	0.030	-0.020 (-0.03)[a]	-
AU				
N_3-H_3···N_1	0.022 (0.024) [b]	0.080	0.002	28.24
N_6-H_6···O_4	0.024 (0.016) [b]	0.098	0.024	6.41
Si···N_1	0.079	0.244	-0.031 (-0.03)[a]	-

[a] Ref [35].
[b] Ref [85].

Earlier studies have found that the finite size of the graphene structure reveals the adsorption spectra in the visible region [78,79]. In the present study, the defective and defect-dopant graphene sheet adsorption regions are calculated at 200-600 nm which are depicted in Figs. 8 and S8, their corresponding optical properties are given in Tables 9, S5 and S6. For DV sheet, the major peaks are observed at 292 nm (HOMO (H)-5→LUMO (L)), whereas the minor peaks are found to be 309 nm (H-6→L), 327 nm (H-1→L+1), 354 nm (H-2→L+1), and 370 nm (H-3→L). While B atom doped with DV sheet, the absorption peak is shifted to a higher wavelength (redshift) at 585 nm (H-2→L). This is because the doping of B atom reduces the ΔE_{HL} value (3.3 eV) between conduction band and valence band, thus the B-DV sheet has higher wavelength this result is quite favoured with FMO and DOS. The Si-DV sheet, the maximum absorption is found to be 308 nm (H-6→L), the minor peaks are obtained at 324 nm (H→L+3), 340 nm (H-2→L+1), and 436 nm (H→L+1). In DV, B and Si doped DV sheet, all these peaks correspond to π-π* transition and this result is well correlated with previous result [51]. The adsorption spectra for SW sheet is obtained at

Table 8
HOMO-LUMO energy gap values are calculated for DNA/RNA base pairs on defective and defect-dopant graphene sheet.

Sheets	Base pairs	HOMO-LUMO energy gap (eV)
DV	-	4.3
	A-T	4.3
DV	G-C	4.2
	A-U	4.3
B-DV	-	3.3
	A-T	3.3
B-DV	G-C	3.1
	A-U	3.3
Si-DV	-	3.8
	A-T	3.8
Si-DV	G-C	3.8
	A-U	3.7
SW	-	4.2
	A-T	4.3
SW	G-C	4.3
	A-U	4.2
B-SW	-	2.5
	A-T	2.6
B-SW	G-C	2.5
	A-U	2.6
Si-SW	-	4.0
	A-T	3.9
Si-SW	G-C	3.7
	A-U	3.8

Table 9
Optical properties are calculated for isolated DNA/RNA base pairs, bare Si-SW sheet and base pair on Si doped SW sheet using TD-DFT by M06-2X/6-311+g* level of theory.

Complex	Wavelength (nm)	Oscillator strength	Excitation energy (eV)	Orbital transition
A-T	230 [220][c]	0.264	5.398 [5.40][a]	H→L+3
	234	0.210	5.280 [5.24][a]	H-1→L
G-C	223	0.426	5.557 [4.75][b]	H→L+11
	236	0.165	5.266	H→L+7
	212	0.131	5.832	H-3→L
A-U	231	0.318	5.357	H→L+3
	225	0.184	5.483	H→L+6
Si-SW	337	0.383	3.672	H-2→L+1
	444	0.221	2.792	H→L+1
	356	0.159	3.479	H-1→L+1
	323	0.085	3.825	H-1→L+1
A-T- Si-SW	494	0.196	2.515	H→L
	348	0.110	3.561	H-1→L+2
	355	0.103	3.481	H-2→L
	381	0.089	3.251	H-1→L
	372	0.054	3.330	H→L+5
G-C Si-SW	482	0.190	2.568	H→L+1
	370	0.125	3.347	H-1→L+1
	354	0.123	3.501	H-1→L+1
	450	0.048	2.751	H-1→L
A-U- Si-SW	497	0.195	2.495	H→L
	354	0.109	3.559	H-1→L

318 nm (H→L+2) (major peak) and the minor peak is calculated at 393 nm (H→L+1). Due to the decreasing ΔE_{HL} value (see Table 8) in B doped SW sheet, the major peak is observed at higher wavelength (444 nm) and their corresponding orbital contributions have occurred at H-5→L. In the case of Si doped sheet SW sheet, the major peak is observed at 337 nm (H-3→L) and their corresponding minor peaks are in 323 nm (H-1→L+2), 356 nm (H-1→L+1), and 444 nm (H→L+1). In the SW, B and Si doped SW sheet the major transition has occurred at π-π*. From the obtained results, it can be observed that the various adsorption peaks in the B-DV and B-SW sheets undergo redshifting (higher wavelength) whereas blue shifting (lower wavelength) are appreciated in the case of Si-DV and Si-SW sheet.

The absorption peaks observed for DNA/RNA base pair on Si-SW sheets are given in Fig. 9 and remaining complex structures are given in Figs. S11-S15. The calculated major absorption peak for A-T and A-U base pair on DV sheet is obtained at 335 nm (H-5→L) and 330 nm (H-4→L), their corresponding minor peaks are obtained at 303 nm (H-8→L) and 305 nm (H-3→L+1), 371 nm (H-4→L) for A-T and 368 nm (H-4→L), 357 nm (H-2→L+1) and 359 nm (H-2→L+1) A-U. For G-C base pair, the maximum absorption peak is calculated at a higher wavelength (374 nm) (H→L+1), similarly, the minor peaks are observed at 328 nm (H-4→L), 365 nm (H-2→L+1), 312 nm (H→L+2), and 345 nm (H-5→L). Among A-T, G-C, and A-U base pair on DV sheet, the maximum wavelength of G-C complex is shifted to red region, due to the smaller E_g value (see Table 8). For A-T, G-C, and A-U on DV sheet, all the orbital transitions are arising from π to π* region. Further, the absorption spectra are calculated for DNA/RNA base pair on B and Si doped DV sheet which is depicted in Figure S6. While comparing with DV complex, the slight changes are monitored in the absorption spectrum of base pair on Si doped DV sheet, the maximum wavelength is found to be 324 nm (H→L+3) for A-T, 339 nm for G-C (H-2→L+1), and 320 nm for A-U. Because the presence of Si atom in DV sheet slightly modifies the electronic properties which are confirmed by FMO and DOS analysis. But in the case of base pair on B doped DV sheet, the absorption peak is highly shifted towards higher wavelength (450 nm) (H-3→L) for A-T, 593 nm (H-1→L) for G-C, and 445 nm (H-3→L) for A-U. The higher wavelength is mainly due to the reduction of ΔE_{HL} value (3.1-3.3 eV). The absorption spectra for the DNA/RNA base pair on SW complexes are illustrated in Figure S6. It can be observed that the major absorption peaks have occurred at 323 nm (H→L+2) for A-T, 321 nm (H→L+2) for A-U, and 327 nm (H→L+2) for G-C. The second major peaks are observed at 399 nm (H→L+1), 398 nm (H→L+1), and 401 nm (H→L+1), these observed peak is main contribution for the orbitals of A-T, G-C and A-U base pair. The B doped SW complex, the major peak is evaluated at 450 (nm) (H-6→L), 437 nm (H-6→L), and 445 nm (H→L+2) for A-T, A-U, and G-C complex. The second peaks at 524 nm (H→L), 527 nm (H→L), and 540 nm (H→L) occur from the orbital transition involving for the DNA/RNA base pair. The higher wavelengths (redshift) in the spectrum of Si doped SW is observed after the adsorption of DNA/RNA base pair. The major peaks are calculated at 494 nm (H→L), 482 nm (H→L), 497 nm (H→L+1) for A-T, A-U, and G-C complex. The higher wavelength is mainly due to the intermolecular interaction between Si and N atom (Si···N). All the orbital transitions are carried out at π-π*. The previous experimental analysis revealed that Si doped graphene sheet improves the sensing properties of molecules [80]. S.K. Mudedla et al [51] have also reported that the Si doped single pentagon and heptagon (57SiGr-L) sheet is adsorbed nucleobases at higher wavelength (374 nm – 557 nm) and this result in good agreement with our present work. From the obtained results, the Si-SW sheet would be expedient in the optical sensing of DNA/RNA constituents.

4. Conclusion

The adsorption strength of DNA/RNA base pair on DV, B-DV, Si-DV, SW, B-SW, and Si-SW graphene sheet has been studied using DFT level of theory. The Si dopant atom present in the SW sheet (Si-SW) substantially increases the adsorption strength of DNA/RNA base pair when compared to bare defective and B doping defective sheet. The highest adsorption strength of DNA/RNA base pair on Si-SW sheet order is found to be -80.59 kcal/mol (G-C) > -70.21 kcal/mol (A-T) > -69.78 kcal/mol (A-U). The highest adsorption energy of DNA/RNA base pairs on Si-SW is due to the partially covalent and partially electrostatic interaction occurred between Si and N atom (Si···N) and π-π stacking interactions and this result in good agreement with the previous study. Examination of results from the topological analysis shows that the nature of interaction between DNA/RNA base pair with DV, B-DV, Si-DV, SW, B-SW, and Si-SW sheet. A positive $\nabla^2\rho(r)$ (0.250 a.u (A-T), 0.030 a.u (G-C), and 0.244 a.u (A-U)) and negative H(r) (-0.031 a.u (A-T), -0.020 a.u (G-C), and -0.031 a.u (A-U)) values showed that the interaction of DNA/RNA base pair on Si-SW sheet has partially electrostatic and partially covalent (Si···N) characters and remaining sheets are adsorbed DNA/RNA base pairs on their surface is in physisorption character, this result in good agreement with reduced density gradient (RDG) analysis. The physisorption interaction and partially covalent and electrostatic interactions do not affect the structure and aromaticity of DNA/RNA base pairs which is confirmed by MCBO analysis. The NPA charge analysis and EDDM strongly reported that the charge is transferred from DNA/RNA base pair to defect and defect-dopant sheet. The charge transfer from N_1/N_3 atom in DNA/RNA base pair to Si-SW sheet is found to be -0.07e eV (A-T), 0.249 eV (G-C), and 0.05 eV for (A-U). Thus, the high adsorption strength and charge transfer mechanism cause significant changes in the electronic structure of Si-SW sheet than the B doped one which is confirmed by DOS analysis. The ΔE_{HL} value of Si-SW sheet undergoes substantial modification after the adsorption of DNA/RNA base pair. These modifications in the ΔE_{HL} value would be mirrored in the conductivity of the intermolecular complexes, thus the Si-SW sheet could be beneficially exploited to design for the fast DNA/RNA sequencing devices and chemical sensing of DNA/RNA base pair. The strong redshift is observed at 482 nm for GC-Si-SW, 494 nm for AT-Si-SW, and 497 nm for AU-Si-SW and this result is well

correlated with previous theoretical study. The obtained results revealed that DNA/RNA base pair on Si-SW surface would be very expedient for the new bio-sensor or DNA/RNA sequencing devices.

Acknowledgements

The authors are thankful to Bharathiar University Research Fellowship (URF) Award no. C2/136/2018 dated: 03.02.2018 for financial assistance.

Appendix A. Supplementary data

Supplementary data to this article can be found online at https://doi.org/10.1016/j.ijbiomac.2020.01.001.

References

[1] J.D. Watson, F.H.C. Crick, Molecular structure of nucleic acids: a structure for deoxyribose nucleic acid, Nature 171 (1953) 737–738, https://doi.org/10.1038/171737a0.
[2] A. Travers, G. Muskhelishvili, DNA structure and function, FEBS J 282 (2015) 2279–2295, https://doi.org/10.1111/febs.13307.
[3] T. Chen, N. Hongdilokkul, Z. Liu, D. Thirunavukarasu, F.E. Romesberg, The expanding world of DNA and RNA, Curr. Opin. Chem. Biol. 34 (2016) 80–87, https://doi.org/10.1016/j.cbpa.2016.08.001.
[4] H. Berney, J. West, E. Haefele, J. Alderman, W. Lane, J.K. Collins, DNA diagnostic biosensor: Development, characterisation and performance, Sensors Actuators, B Chem 68 (2000) 100–108, https://doi.org/10.1016/S0925-4005(00)00468-8.
[5] O. Akhavan, E. Ghaderi, R. Rahighi, Toward Single-DNA Electrochemical Biosensing by graphene nanowalls, ACS Nano 6 (2012) 2904–2916, https://doi.org/10.1021/nn300261t.
[6] Y. Liu, X. Dong, P. Chen, Biological and chemical sensors based on graphene materials, Chem. Soc. Rev. 41 (2012) 2283–2307, https://doi.org/10.1039/c1cs15270j.
[7] F. Lu, S. Zhang, H. Gao, H. Jia, L. Zheng, Protein-decorated reduced oxide graphene composite and its application to SERS, ACS Appl. Mater. Interfaces. 4 (2012) 3278–3284, https://doi.org/10.1021/am300634n.
[8] Y. Lu, M.B. Lerner, Z. John Qi, J.J. Mitala, J. Hsien Lim, B.M. Discher, A.T. Charlie Johnson, Graphene-protein bioelectronic devices with wavelength-dependent photoresponse, Appl. Phys. Lett. 100 (2012) 2012–2015, https://doi.org/10.1063/1.3678024.
[9] L.G. Ee, L.J. Li, K. Zhang, Y. Xu, X. Dong, X. Ho, S.L. Pooi, J. Kasim, Z.X. Shen, J.A. Rogers, S.G. Mhaisalkar, DNA sensing by field-effect transistors based on networks of carbon nanotubes, J. Am. Chem. Soc. 129 (2007) 14427–14432, https://doi.org/10.1021/ja075176g.
[10] B. Luan, R. Zhou, Nanopore-based sensors for detecting toxicity of a carbon nanotube to proteins, J. Phys. Chem. Lett. 3 (2012) 2337–2341, https://doi.org/10.1021/jz3007832.
[11] M. Calvaresi, F. Zerbetto, The Devil and Holy Water: Protein and Carbon Nanotube Hybrids, Acc. Chem. Res. 46 (2013) 2454–2463, https://doi.org/10.1021/ar300347d.
[12] Y. Xuan, Y.Q. Wu, T. Shen, M. Qi, M.A. Capano, J.A. Cooper, P.D. Ye, Atomic-layer-deposited nanostructures for graphene-based nanoelectronics, Appl. Phys. Lett. 92 (2008) 2006–2009, https://doi.org/10.1063/1.2828338.
[13] X. Yang, Y. Tu, L. Li, S. Shang, X.M. Tao, Well-dispersed chitosan/graphene oxide nanocomposites, ACS Appl. Mater. Interfaces. 2 (2010) 1707–1713, https://doi.org/10.1021/am100222m.
[14] C. Liu, S. Alwarappan, Z. Chen, X. Kong, C.Z. Li, Membraneless enzymatic biofuel cells based on graphene nanosheets, Biosens. Bioelectron. 25 (2010) 1829–1833, https://doi.org/10.1016/j.bios.2009.12.012.
[15] X. Li, X. Wang, L. Zhang, S. Lee, H. Dai, Chemically derived, ultrasmooth graphene nanoribbon semiconductors, Science (80-.) 319 (2008) 1229–1232, https://doi.org/10.1126/science.1150878.
[16] C.C. Lu, Y.C. Lin, C.H. Yeh, J.C. Huang, P.W. Chiu, High mobility flexible graphene field-effect transistors with self-healing gate dielectrics, ACS Nano 6 (2012) 4469–4474, https://doi.org/10.1021/nn301199j.
[17] M.D. Stoller, S. Park, Y. Zhu, J. An, R.S. Ruoff, Graphene-Based ultracapacitors, Nano Lett 8 (2008) 3498–3502, https://doi.org/10.1021/nl802558y.
[18] W. Qin, X. Li, W.W. Bian, X.J. Fan, J.Y. Qi, Density functional theory calculations and molecular dynamics simulations of the adsorption of biomolecules on graphene surfaces, Biomaterials 31 (2010) 1007–1016, https://doi.org/10.1016/j.biomaterials.2009.10.013.
[19] H.E. Romero, P. Joshi, A.K. Gupta, H.R. Gutierrez, M.W. Cole, S.A. Tadigadapa, P.C. Eklund, Adsorption of ammonia on graphene, Nanotechnology 20 (2009) https://doi.org/10.1088/0957-4484/20/24/245501.
[20] R. Akilan, M. Malarkodi, S. Vijayakumar, S. Gopalakrishnan, R. Shankar, Modeling of 2-D hydrogen-edge capped defected & boron-doped defected graphene sheets for the adsorption of CO2, SO2 towards energy harvesting applications, Appl. Surf. Sci. 463 (2019) 596–609, https://doi.org/10.1016/j.apsusc.2018.08.179.
[21] B.S. Husale, S. Sahoo, A. Radenovic, F. Traversi, P. Annibale, A. Kis, SsDNA binding reveals the atomic structure of graphene, Langmuir 26 (2010) 18078–18082, https://doi.org/10.1021/la102518t.
[22] C.H. Lu, J. Li, X.L. Zhang, A.X. Zheng, H.H. Yang, X. Chen, G.N. Chen, General approach for monitoring peptide-protein interactions based on graphene-peptide complex, Anal. Chem. 83 (2011) 7276–7282, https://doi.org/10.1021/ac200617k.
[23] Y. Weizmann, D.M. Chenoweth, T.M. Swager, DNA-CNT nanowire networks for DNA detection, J. Am. Chem. Soc. 133 (2011) 3238–3241, https://doi.org/10.1021/ja109180d.
[24] X. Liu, F. Wang, R. Aizen, O. Yehezkeli, I. Willner, Graphene oxide/nucleic-acid-stabilized silver nanoclusters: Functional hybrid materials for optical aptamer sensing and multiplexed analysis of pathogenic DNAs, J. Am. Chem. Soc. 135 (2013) 11832–11839, https://doi.org/10.1021/ja403485r.
[25] S.M. Maliyekkal, T.S. Sreeprasad, D. Krishnan, S. Kouser, A.K. Mishra, U.V. Waghmare, T. Pradeep, Graphene: A reusable substrate for unprecedented adsorption of pesticides, Small 9 (2013) 273–283, https://doi.org/10.1002/smll.201201125.
[26] K. Balamurugan, V. Subramanian, Adsorption of chlorobenzene onto (5,5) armchair single-walled carbon nanotube and graphene sheet: Toxicity versus adsorption strength, J. Phys. Chem. C. 117 (2013) 21217–21227, https://doi.org/10.1021/jp403646h.
[27] N. Mohanty, V. Berry, Graphene-based single-bacterium resolution biodevice and DNA transistor: Interfacing graphene derivatives with nanoscale and microscale biocomponents, Nano Lett 8 (2008) 4469–4476, https://doi.org/10.1021/nl802412n.
[28] J. Dai, J. Yuan, P. Giannozzi, Gas adsorption on graphene doped with B, N, Al, and S: A theoretical study, Appl. Phys. Lett. 95 (2009) https://doi.org/10.1063/1.3272008.
[29] Z.M. Ao, S. Li, Q. Jiang, Correlation of the applied electrical field and CO adsorption/desorption behavior on Al-doped graphene, Solid State Commun 150 (2010) 680–683, https://doi.org/10.1016/j.ssc.2009.12.016.
[30] X. Kong, Q. Chen, Z. Sun, Enhanced oxygen reduction reactions in fuel cells on H-decorated and B-substituted graphene, ChemPhysChem 14 (2013) 514–519, https://doi.org/10.1002/cphc.201200918.
[31] W. Sun, Y. Bu, Y. Wang, Interaction between glycine/glycine radicals and intrinsic/boron-doped (8,0) single-walled carbon nanotubes: A density functional theory study, J. Phys. Chem. B. 112 (2008) 15442–15449, https://doi.org/10.1021/jp804965x.
[32] S. Agnoli, M. Favaro, Doping graphene with boron: A review of synthesis methods, physicochemical characterization, and emerging applications, J. Mater. Chem. A. 4 (2016) 5002–5025, https://doi.org/10.1039/c5ta10599d.
[33] Y. Chen, Y.J. Liu, H.X. Wang, J.X. Zhao, Q.H. Cai, X.Z. Wang, Y.H. Ding, Silicon-doped graphene: An effective and metal-free catalyst for NO reduction to N2O? ACS Appl. Mater. Interfaces. 5 (2013) 5994–6000, https://doi.org/10.1021/am400563g.
[34] Y. Zou, F. Li, Z.H. Zhu, M.W. Zhao, X.G. Xu, X.Y. Su, An ab initio study on gas sensing properties of graphene and Si-doped graphene, Eur. Phys. J. B 81 (2011) 475–479, https://doi.org/10.1140/epjb/e2011-20225-8.
[35] Y. Chen, B. Gao, J.X. Zhao, Q.H. Cai, H.G. Fu, Si-doped graphene: an ideal sensor for NO- or NO2-detection and metal-free catalyst for N2O-reduction, J. Mol. Model. 18 (2012) 2043–2054, https://doi.org/10.1007/s00894-011-1226-x.
[36] S.K. Mudedla, K. Balamurugan, V. Subramanian, Computational study on the interaction of modified nucleobases with graphene and doped graphenes, J. Phys. Chem. C. 118 (2014) 16165–16174, https://doi.org/10.1021/jp503126q.
[37] D.H. Lim, A.S. Negreira, J. Wilcox, DFT studies on the interaction of defective graphene-supported Fe and Al nanoparticles, J. Phys. Chem. C. 115 (2011) 8961–8970, https://doi.org/10.1021/jp2012914.
[38] Z. Xu, B.R. Meher, D. Eustache, Y. Wang, Insight into the interaction between DNA bases and defective graphenes: Covalent or non-covalent, J. Mol. Graph. Model. 47 (2014) 8–17, https://doi.org/10.1016/j.jmgm.2013.10.007.
[39] D. Borisova, V. Antonov, A. Proykova, Hydrogen sulfide adsorption on a defective graphene, Int. J. Quantum Chem. 113 (2013) 786–791, https://doi.org/10.1002/qua.24077.
[40] B. Sanyal, O. Eriksson, U. Jansson, H. Grennberg, Molecular adsorption in graphene with divacancy defects, Phys. Rev. B. 79 (2009) 1–4, https://doi.org/10.1103/physrevb.79.113409.
[41] Y.H. Zhang, K.G. Zhou, K.F. Xie, X.C. Gou, J. Zeng, H.L. Zhang, Y. Peng, Effects of stone-wales defect on the interactions between NH3, NO2 and graphene, J. Nanosci. Nanotechnol. 10 (2010) 7347–7350, https://doi.org/10.1166/jnn.2010.2929.
[42] X. Qin, Q. Meng, W. Zhao, Effects of Stone-Wales defect upon adsorption of formaldehyde on graphene sheet with or without Al dopant: A first principle study, Surf. Sci. 605 (2011) 930–933, https://doi.org/10.1016/j.susc.2011.02.006.
[43] Y. Zhao, D.G. Truhlar, The M06 suite of density functionals for main group thermochemistry, thermochemical kinetics, noncovalent interactions, excited states, and transition elements: two new functionals and systematic testing of four M06-class functionals and 12 other function, Theor. Chem. Acc. 120 (2008) 215–241, https://doi.org/10.1007/s00214-007-0310-x.
[44] J.-D. Chai, M. Head-Gordon, Systematic optimization of long-range corrected hybrid density functionals, J. Chem. Phys. 128 (2008), 084106. https://doi.org/10.1063/1.2834918.
[45] J.C. and D.J.F. M. J. Frisch, G. W. Trucks, H. B. Schlegel, G. E. Scuseria, M. A. Robb, J. R. Cheeseman, G. Scalmani, V. Barone, B. Mennucci, G. A. Petersson, H. Nakatsuji, M. Caricato, X. Li, H. P. Hratchian, A. F. Izmaylov, J. Bloino, G. Zheng, J. L. Sonnenberg, M, Gaussian 09, (2009).
[46] S.F. Boys, F. Bernardi, The calculation of small molecular interactions by the differences of separate total energies. Some procedures with reduced errors, Mol. Phys. 19 (1970) 553–566, https://doi.org/10.1080/00268977000101561.
[47] J. Antony, S. Grimme, Structures and interaction energies of stacked graphene–nucleobase complexes, Phys. Chem. Chem. Phys. 10 (2008) 2722, https://doi.org/10.1039/b718788b.

[48] S. Vinnarasi, R. Radhika, S. Vijayakumar, R. Shankar, Structural insights into the anticancer activity of quercetin on G-tetrad, mixed G-tetrad, and G-quadruplex DNA using quantum chemical and molecular dynamics simulations, J. Biomol. Struct. Dyn. 0 (2019) 1–23. doi:https://doi.org/10.1080/07391102.2019.1574239.
[49] S. Wang, B. Yang, J. Yuan, Y. Si, H. Chen, Large-Scale Molecular Simulations on the Mechanical Response and Failure Behavior of a defective graphene: Cases of 5-8-5 Defects, Sci. Rep. 5 (2015) 1–9, https://doi.org/10.1038/srep14957.
[50] O. Brovarets, D. Hovorun, Surprising conformers of the biologically important A·T DNA base pairs: QM/QTAIM proofs, Front. Chem. 6 (2018) 1–11, https://doi.org/10.3389/fchem.2018.00008.
[51] S.K. Mudedla, K. Balamurugan, M. Kamaraj, V. Subramanian, Interaction of nucleobases with silicon doped and defective silicon doped graphene and optical properties, Phys. Chem. Chem. Phys. 18 (2016) 295–309, https://doi.org/10.1039/c5cp06059a.
[52] M. Endo, T. Hayashi, S.H. Hong, T. Enoki, M.S. Dresselhaus, Scanning tunneling microscope study of boron-doped highly oriented pyrolytic graphite, J. Appl. Phys. 90 (2001) 5670–5674, https://doi.org/10.1063/1.1409581.
[53] R.H. Miwa, T.B. Martins, A. Fazzio, Hydrogen adsorption on boron doped graphene: an ab initio study, Nanotechnology 19 (2008) https://doi.org/10.1088/0957-4484/19/15/155708.
[54] H.R. Drew, R.M. Wingtt, T. Takanot, C. Brokat, S. Tanakat, K. Itakuraii, R.E. Dickersont, Structure of a B-DNA dodecamer: Conformation and dynamics * Biochemistry, Proc. Natl. Acad. Sci. 78 (1981) 2179–2183.
[55] S. Perun, A.L. Sobolewski, W. Domcke, Ab initio studies of the photophysics of 2-aminopurine, Mol. Phys. 104 (2006) 1113–1121, https://doi.org/10.1080/00268970500417341.
[56] T. Marino, N. Russo, M. Toscano, M. Pavelka, Theoretical investigation on DNA/RNA base pairs mediated by copper, silver, and gold cations, Dalton Trans. 41 (2012) 1816–1823, https://doi.org/10.1039/C1DT11028D.
[57] D. Cortés-Arriagada, Phosphorene as a Template Material for physisorption of DNA/RNA nucleobases and Resembling of Base Pairs: A Cluster DFT Study and Comparisons with graphene, J. Phys. Chem. C. 122 (2018) 4870–4880, https://doi.org/10.1021/acs.jpcc.7b11268.
[58] N. Varghese, U. Mogera, A. Govindaraj, A. Das, P.K. Maiti, A.K. Sood, C.N.R. Rao, Binding of DNA nucleobases and nucleosides with graphene, ChemPhysChem 10 (2009) 206–210, https://doi.org/10.1002/cphc.200800459.
[59] S. Chandra Shekar, R.S. Swathi, Stability of nucleobases and base pairs adsorbed on graphyne and graphdiyne, J. Phys. Chem. C. 118 (2014) 4516–4528, https://doi.org/10.1021/jp412791v.
[60] P. Hobza, J. Šponer, Structure, Energetics, and Dynamics of the Nucleic acid base Pairs: Nonempirical ab Initio Calculations, Chem. Rev. 99 (1999) 3247–3276.
[61] Z.E. Hughes, G. Wei, K.L.M. Drew, L. Colombi Ciacchi, T.R. Walsh, Adsorption of DNA Fragments at Aqueous Graphite and Au(111) via Integration of Experiment and Simulation, Langmuir 33 (2017) 10193–10204, https://doi.org/10.1021/acs.langmuir.7b02480.
[62] A. Das, A.K. Sood, P.K. Maiti, M. Das, R. Varadarajan, C.N.R. Rao, Binding of nucleobases with single-walled carbon nanotubes: Theory and experiment, Chem. Phys. Lett. 453 (2008) 266–273, https://doi.org/10.1016/j.cplett.2008.01.057.
[63] A. Gourishankar, S. Shukla, K.N. Ganesh, M. Sastry, Isothermal Titration calorimetry Studies on the Binding of DNA Bases and PNA base Monomers to Gold Nanoparticles, J. Am. Chem. Soc. 126 (2004) 13186–13187, https://doi.org/10.1021/ja046785g.
[64] M. Rastgoo, M. Fathipour, Interaction of DNA nucleobases with boron, nitrogen, and sulfur doped graphene nano-ribbon for sequencing: an Ab initio study, Appl. Surf. Sci. 492 (2019) 634–643, https://doi.org/10.1016/j.apsusc.2019.06.208.
[65] Q. Lin, X. Zou, G. Zhou, R. Liu, J. Wu, J. Li, W. Duan, Adsorption of DNA/RNA nucleobases on hexagonal boron nitride sheet: an ab initio study, Phys. Chem. Chem. Phys. 13 (2011) 12225–12230, https://doi.org/10.1039/c1cp20783k.
[66] R. Parthasarathi, V. Subramanian, N. Sathyamurthy, Hydrogen Bonding without borders: an Atoms-in-Molecules Perspective, J. Phys. Chem. A. 110 (2006) 3349–3351, https://doi.org/10.1021/jp060571z.
[67] M. Giambiagi, M.S. De Giambiagi, C.D. Dos Santos Silva, A.P. De Figueiredo, Multicenter bond indices as a measure of aromaticity, Phys. Chem. Chem. Phys. 2 (2000) 3381–3392, https://doi.org/10.1039/b002009p.
[68] P. Bultinck, R. Ponec, S. Van Damme, Multicenter bond indices as a new measure of aromaticity in polycyclic aromatic hydrocarbons, J. Phys. Org. Chem. 18 (2005) 706–718, https://doi.org/10.1002/poc.922.
[69] E.R. Johnson, S. Keinan, P. Mori-Sánchez, J. Contreras-García, A.J. Cohen, W. Yang, Revealing Noncovalent Interactions, J. Am. Chem. Soc. 132 (2010) 6498–6506, https://doi.org/10.1021/ja100936w.
[70] J.H. Lee, Y.K. Choi, H.J. Kim, R.H. Scheicher, J.H. Cho, Physisorption of DNA nucleobases on h -BN and graphene: VdW-corrected DFT calculations, J. Phys. Chem. C. 117 (2013) 13435–13441, https://doi.org/10.1021/jp402403f.
[71] S.K. Min, W.Y. Kim, Y. Cho, K.S. Kim, Fast DNA sequencing with a graphene-based nanochannel device, Nat. Nanotechnol. 6 (2011) 162–165, https://doi.org/10.1038/nnano.2010.283.
[72] S.J. Heerema, C. Dekker, Graphene nanodevices for DNA sequencing, Nat. Nanotechnol. 11 (2016) 127–136, https://doi.org/10.1038/nnano.2015.307.
[73] A. Ambrosi, M. Pumera, Stacked graphene nanofibers for electrochemical oxidation of DNA bases, Phys. Chem. Chem. Phys. 12 (2010) 8943–8947, https://doi.org/10.1039/c0cp00213e.
[74] Y. Cho, S.K. Min, W.Y. Kim, K.S. Kim, The origin of dips for the graphene-based DNA sequencing device, Phys. Chem. Chem. Phys. 13 (2011) 14293–14296, https://doi.org/10.1039/c1cp20760a.
[75] E.M. Evertsz, K. Rippe, T.M. Jovin, Parallel-stranded duplex DNA containing blocks of trans purine-purine and purine-pyrimidine base pairs, Nucleic Acids Res 22 (1994) 3293–3303, https://doi.org/10.1093/nar/22.16.3293.
[76] M.K. Shukla, J. Leszczynski, A theoretical study of excited state properties of adenine - thymine and guanine - cytosine base pairs, J. Phys. Chem. A. 106 (2002) 4709–4717, https://doi.org/10.1021/jp014516w.
[77] S. Saha, H.M. Quiney, Solvent effects on the excited state characteristics of adenine-thymine base pairs, RSC Adv 7 (2017) 33426–33440, https://doi.org/10.1039/c7ra03244g.
[78] H. Vovusha, B. Sanyal, DFT and TD-DFT studies on the electronic and optical properties of explosive molecules adsorbed on boron nitride and graphene nano flakes, RSC Adv 5 (2015) 4599–4608, https://doi.org/10.1039/c4ra11314d.
[79] H. Vovusha, S. Sanyal, B. Sanyal, Interaction of nucleobases and aromatic amino acids with graphene oxide and graphene flakes, J. Phys. Chem. Lett. 4 (2013) 3710–3718, https://doi.org/10.1021/jz401929h.
[80] R. Lv, M.C. Dos Santos, C. Antonelli, S. Feng, K. Fujisawa, A. Berkdemir, A.L. Elías, N. Perea-Lopez, M. Terrones, R. Cruz-Silva, F. López-Urías, H. Terrones, Large-area si-doped graphene: Controllable synthesis and enhanced molecular sensing, Adv. Mater. 26 (2014) 7593–7599, https://doi.org/10.1002/adma.201403537.
[81] R. Shankar, R. Radhika, D. Thangamani, L. Senthil Kumar, P. Kolandaivel, Theoretical studies on interaction of anticancer drugs (dacarbazine, procarbazine and triethylenemelamine) with normal (AT and GC) and mismatch (GG, CC, AA and TT) base pairs, Mol. Simul. 41 (2015) 633–652, https://doi.org/10.1080/08927022.2014.913098.
[82] J. Šponer, J. Leszczynski, P. Hobza, Structures and Energies of Hydrogen-Bonded DNA base Pairs. A Nonempirical Study with Inclusion of electron Correlation, J. Phys. Chem. 100 (1996) 1965–1974, https://doi.org/10.1021/jp952760f.
[83] L. Li, D. Peng, X. Chen, L. Liu, A. Tian, Theoretical investigation on the adsorption of DNA bases on B/N-doped SWCNT surface by the first principle, AIP Adv 7 (2017), 105004. https://doi.org/10.1063/1.4983482.
[84] M. Lukas, R.E.A. Kelly, L.N. Kantorovich, R. Otero, W. Xu, E. Laegsgaard, I. Stensgaard, F. Besenbacher, Adenine monolayers on the Au(111) surface: Structure identification by scanning tunneling microscopy experiment and ab initio calculations, J. Chem. Phys. 130 (2009), 024705. https://doi.org/10.1063/1.3046690.
[85] P. R, et al., R. Amutha; V. Subramanian, Balachandran Unni Nair, T. Ramasami, Bader's and Reactivity Descriptors' Analysis of DNA Base Pairs, J. Phys. Chem. A 108 (17) (2004) 3817–3828, https://doi.org/10.1021/jp031285f.